THESIS FOR THE DEGREE OF LICENTIATE

Squeezed state generation in silicon nitride microring resonators

Sara Persia

Photonics Laboratory
Department of Microtechnology and Nanoscience (MC2)
Chalmers University of Technology
Göteborg, Sweden, 2026

Squeezed state generation in silicon nitride microring resonators

Sara Persia

Göteborg, February 2026

ISSN 1652-0769
Technical Report MC2-476

Photonics Laboratory
Department of Microtechnology and Nanoscience (MC2)
Chalmers University of Technology
SE–412 96 Göteborg, Sweden
Telephone: +46 (0)31–772 10 00

Printed in Sweden by
Reproservice
Chalmers Tekniska Högskola
Göteborg, Sweden, 2026

Squeezed state generation in silicon nitride microring resonators

Sara Persia
Photonics Laboratory
Department of Microtechnology and Nanoscience (MC2)
Chalmers University of Technology

Abstract

Squeezed states, with their noise reduction below the standard quantum limit, are promising quantum states of light exploited for enhancing sensitivity in quantum sensing or as carriers of information in continuous variable quantum computing and communication. To make use of their quantum advantage, the main common challenge in generating these states is achieving high levels of squeezing in low loss setups.

Over the years, several bulk optical nonlinear crystals and cavities have been employed for the generation of different types of high-quality squeezed states. However, recent progress in fabricating ultra-low loss integrated waveguides has shifted the interest of the community towards the integration of squeezing sources to gain advantages in terms of compactness, scalability, and reproducibility.

The aim of this thesis is to investigate the main characteristics, limits, and requirements for the generation of vacuum and bright squeezed states by second- and third-order nonlinear devices, with more emphasis on integrated cavities. In particular, we demonstrate high on-chip intensity difference squeezing between bright mode pairs created in an engineered SiN microring resonator. In addition, we propose the use of the Ikeda map, a semi-classical simulation tool, for the investigation of two-mode quadrature squeezing generation in microresonators, discussing its competitiveness against standard quantum models. These results contribute to the optimization of engineered integrated devices with the aim of attaining high levels of squeezing sufficient to bring real advantages in classical and quantum applications.

Keywords: squeezed states, intensity difference squeezing, squeezing simulations, microring resonators, nonlinear integrated photonics

Publications

This thesis is based on the work contained in the following papers and conference contributions:

[A] Sara Persia, Yi Sun, Vaishali Adya, and Victor Torres-Company, "Intensity difference squeezing of high-power modes in a strongly overcoupled silicon nitride microresonator", *Submitted to Optics Letters, 2026.*

[B] Sara Persia, Fuchuan Lei, Vaishali Adya, and Victor Torres-Company, "Semi-classical analysis of two-mode quadrature squeezing in a high-Q microresonator", *Submitted to Conference on Lasers and Electro-Optics (CLEO), 2026*

Contents

Acknowledgement

I would like to start by expressing my gratitude to my main supervisor, Prof. Victor Torres Company, for his endless support in this shared journey into quantum photonics. His knowledge, guidance, and encouragement helped me grow both as a researcher and as a human being. Thank you to my co-supervisor, Prof. Vaishali Adya, for sharing with me her immense knowledge about squeezing. I am grateful to the professors Peter Andrekson, Magnus Karlsson, Raphaël Van Laer, and my examiner, Åsa Haglund, for their support and for making the Photonics Lab an excellent academic environment.

I am also very thankful to Dr. Fuchuan Lei, Dr. Óskar Bjarki Helgason, Dr. Krishna Sundar Twayana, and Dr. Yan Gao for helping me understand the classical dynamics of microring resonators, both in the lab and through simulations. I also thank Dr. Marcello Girardi for teaching me the fabrication process, and Dr. Israel Rebolledo Salgado for his help in the lab and for the amazing Mexican dinners. I would also like to thank Tim Fuhrmann, Niklas Hammerschmidt, Vijay Shekhawat, Yi Sun, Mia Buchmayr, Dr. Yvan Klaver, Dr. Kaiyi Wu, and Dr. Xiaomin Lyu for the wonderful atmosphere you create in the group, making it possible to share knowledge and challenges, and to celebrate our successes together. I extend my thanks to the entire Photonics Lab and to everyone at WACQT.

Special thanks go to Estrella, Núria, and Carmen for their beautiful friendship, the immense support, and the special moments spent together these years. Thank you, Ruggero, for always being there with your love and endless support.

Finally, my deepest gratitude goes to my family. Everything I have achieved has been possible only because of your love and encouragement. Thank you for always believing in me.

Acronyms

BPD	balanced photodetector
CV	continuous variable
CW	continuous wave
EO	electro-optic
ESA	electrical spectrum analyzer
FSR	free spectral range
FWM	four-wave mixing
GBS	Gaussian boson sampling
GKP	Gottesman-Kitaev-Preskil
LIGO	laser interferometer gravitational wave observatory
LO	local oscillator
NLSE	nonlinear Schrödinger equation
OPA	optical parametric amplifier
OPO	optical parametric oscillator
OSA	optical spectrum analyzer
PICs	photonic integrated circuits
quasi-BICs	quasi-bound states in the continuum
SNR	signal-to-noise ratio
SPM	self-phase modulation
TWM	three-wave mixing
VOA	variable optical attenuator
XPM	cross-phase modulation

Chapter 1

Introduction

1.1 Historical background

The quantum theory of light is necessary to explain optical phenomena at the most fundamental level. The origins of quantum optics date back to the development of quantum mechanics itself. In 1900, Max Planck introduced the concept of quantized energy in the atomic emission and absorption of light while addressing the black-body radiation problem. Five years later, Albert Einstein introduced the concept of quanta of light, later called photons, to explain the photoelectric effect. In 1909, Einstein further described for the first time the wave–particle duality of light. This concept was formally described within the framework of quantum mechanics by Paul Dirac in 1927, when he introduced the creation and annihilation operators. These developments lay the foundation of the modern quantum theory of light, opening the door to new concepts and phenomena that cannot be described by a semiclassical theory.

In classical optics, the wave nature of light is represented by Maxwell's equations describing the electromagnetic fields. In the quantum theory of light, instead, the particle nature of light arises from the quantized virtual harmonic oscillators used to describe the fields. One of the first important concepts arising from this quantum description is the existence of the zero-point energy fluctuations, also called quantum or vacuum fluctuations [1]. It is now known that vacuum fluctuations are fundamental to explain many quantum effects and phenomena [1], such as the Casimir effect, the Lamb effect, and the spontaneous emission process driven by vacuum fluctuations. More importantly, vacuum fluctuations are at the origin of what is usually called quantum noise.

The Heisenberg uncertainty principle describes the important properties of the quantum noise that affect every quantum state of light. It poses a limit to the total uncertainty of two conjugate variables. A quantum state with the minimum total quantum noise, distributed equally among the field quadratures, is the coherent state, which is the closest quantum description to a classical laser beam. In case of zero mean amplitude, such a state is defined as a vacuum state [2]. The quantum noise properties of these light states significantly affect the fundamental noise limits and the intrinsic functions of many classical and quantum optical devices. Recent developments in classical and quantum optics have pushed the device performances to a level where the quantum noise is the ultimate limiting factor. Going beyond these limits requires the use of particular quantum states of light with peculiar noise properties, such as squeezed states, or NOON states [3].

Squeezed states

Squeezed states are among the simplest types of quantum states that can be generated from a classical coherent laser by exploiting non-linear effects in optical devices. The unique properties of squeezed states rely on the distribution of their quantum noise. A squeezed state exhibits reduced noise in one variable compared to the vacuum noise level, at the expense of increased noise in the corresponding conjugate variable [4, 5].

The first mathematical descriptions of squeezed states were developed in the early 1970s by several researchers [6–8]. However, significant interest of the scientific community emerged only after the proposal of C. M. Caves in 1981 to use squeezed states in the detection of gravitational waves [9]. These works highlighted the crucial role that squeezed states could have in all experiments limited by the noise performances of the optical devices. Squeezed states could lower these limits, increase measurement sensitivity, and signal-to-noise ratio [10]. The first experimental demonstration of squeezing generation arrived in the mid-1980s, when R. E. Slusher *et al.* measured 3 dB of amplitude squeezing produced from the non-linear four-wave mixing (FWM) process in sodium vapor inside a bulk optical cavity [11]. Since then, substantial effort has been directed towards increasing the achievable squeezing level, exploring new generation sources, and improving the measurement techniques.

During the 1990s and 2000s, advances in nonlinear crystals, optical fiber-based cavities, and low-loss detection techniques enabled the realization of stronger and more stable squeezing sources [12–17]. In these

years, optical parametric oscillators (OPOs) and optical parametric amplifiers (OPAs) became the dominant platforms for generating squeezed states through non-linear processes such as FWM or parametric down conversion (PDC). To date, the highest measured squeezing level of 15 dB has been obtained from a second-order nonlinear crystal in a doubly resonant OPA [18].

So far, the most relevant and well-known use of squeezed states is the detection of gravitational waves performed by the LIGO community. They exploit state-of-the-art optical equipment to develop frequency-tunable squeezing able to enhance the detection sensitivity over a broad frequency range [19,20]. Following their path, further developments have been achieved in the field of quantum sensing with the introduction of squeezed states [21–25]. Beyond sensing applications, squeezed states represent a fundamental building block in quantum information processing [26]. They can be used as basic elements in quantum simulators [27, 28], as well as in continuous- and discrete-variable quantum computing, either directly as quantum modes (qumodes) or as sources to generate more complex quantum states and qubits [29–32].

In the last few decades, the improvements made in integrated photonic circuits have shifted the interest of squeezing generation towards miniaturized devices. Photonic integrated circuits (PICs) offer key advantages in terms of scalability, small-footprint, and reduced power consumption, becoming attractive platforms for new generations of quantum technologies [33]. In this context, the main platforms used to generate squeezing are thin film lithium niobate waveguides [34–36] and silicon nitride microring resonators [37–40], due to their low loss and high nonlinearity, essential requirements for squeezing generation.

It is worth noticing that the requirements of the generated squeezed states vary across the different platforms depending on the target application. Several types of squeezed states with different properties can be obtained in these PICs, such as broadband single-mode squeezing [41], intensity difference squeezing [42], and integrated squeezed frequency combs [43]. Nevertheless, achieving the highest possible squeezing level is still the main common requirement. At the same time, this represents the main significant challenge across all integrated platforms, mainly due to the system loss imposed by the fabrication limits. The highest on-chip squeezing levels archived so far are 12 dB in thin film lithium niobate [36] and 10 dB in engineered silicon nitride microring resonators [42, 44]. To obtain even higher squeezing levels in integrated optics, new ways to

reduce losses are required.

Squeezed states are not yet used in commercial applications, especially because any optical loss in the system degrades the squeezing quality, effectively transforming the squeezed state into a coherent state and eliminating its quantum advantage. Nonetheless, squeezed states continue to play a fundamental role in quantum optics research.

1.2 This thesis

This thesis focuses on the analysis of squeezed state generation in SiN integrated microring resonators to investigate and overcome the limiting factors in achieving high squeezing levels. The generation of two different types of squeezed states in engineered devices is analyzed using an unconventional simulation tool and through experiments.

In Paper A, intensity difference squeezing between bright twin beams is measured. The paired modes are generated in a silicon nitride microresonator through the FWM process driven by a strong input pump laser operating above the oscillation threshold. The device is engineered to give rise to quasi-bound states in the continuum (quasi-BICs) [45], which provide optimal conditions for high on-chip squeezing generation.

In Paper B, a semi-classical simulation tool, based on methods typically used to model the classical behavior of the microring resonators, is implemented to analyze squeezing generation. In particular, two-mode quadrature squeezing arising in microresonators operated below the parametric oscillation threshold is simulated over several mode pairs, both in the time and in the frequency domain.

Thesis outline

The thesis is organized as follows. Chapter 2 gives an introduction to the fundamental concepts of vacuum and squeezed states, along with their quantum noise properties. Chapter 3 discusses the nonlinear processes commonly used to generate squeezed states in OPOs and OPAs. Chapter 4 provides an overview of the different types of squeezed states that can be generated in both bulk and integrated OPOs and OPAs. A brief description of the main applications in the field of quantum information processing is also presented. Then, Chapter 5 describes the semi-classical simulation tool and the linear dynamics of the engineered microring resonators used in Papers A and B. Finally, Chapter 6 presents the thesis summary and future outlook.

Chapter 2

Squeezed states

The aim of this thesis is to investigate the generation of a particular class of quantum states, i.e., squeezed states, in integrated photonic devices. These states exhibit unequal quantum noise properties, and this Chapter aims to provide an overview of the fundamental concepts necessary to fully comprehend their unique properties. In particular, in the following sections, we focus on an intuitive description of quantum noise and how it is manipulated in a squeezed state.

2.1 Quantum noise

2.1.1 From classical to quantum noise

In classical optics, a monochromatic light beam is described by a time-dependent electromagnetic field. In the ideal case, its optical spectrum is composed of a single frequency component ν_0, or angular frequency $\omega_0 = 2\pi\nu_0$, with non-zero intensity. At a fixed point in space, this field is a pure time-dependent sinusoid. The electromagnetic field is usually described by a complex amplitude α_0 and a phase term ϕ, or equivalently in terms of the quadrature-phase amplitudes X_1 and X_2, representing the real and imaginary components of the field [46]:

$$\begin{aligned} E(\mathbf{r},t) &= E_0[\alpha_0(\mathbf{r},t)e^{-i(\omega t+\phi(\mathbf{r},t))} + \alpha_0^*(\mathbf{r},t)e^{i(\omega t+\phi(\mathbf{r},t))}] = \\ &= E_0[X_1(\mathbf{r},t)\cos(\omega t) + X_2(\mathbf{r},t)\sin(\omega t)]. \end{aligned} \tag{2.1}$$

A typical graphical representation of the field is in a phasor diagram, where the electromagnetic wave is represented by a vector in the quadrature-phase amplitudes plane. The distance of the point-like end of

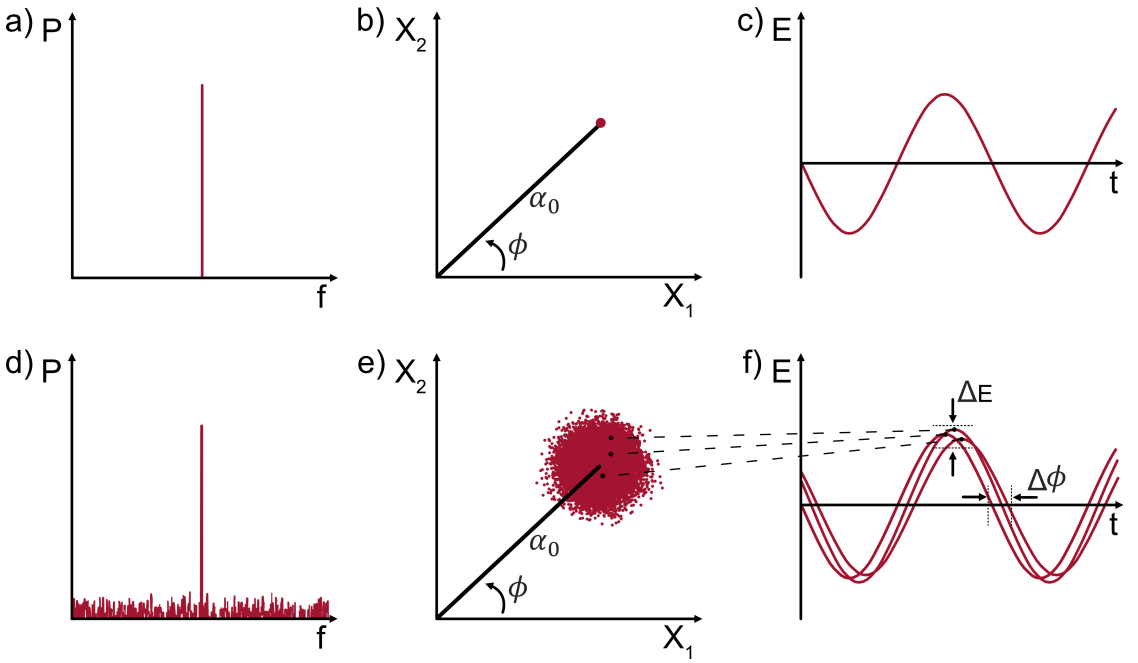

Figure 2.1: Graphical representations of an ideal monochromatic light beam (first row) and of a real beam subject to fluctuations (second row). a) In the ideal case, the optical spectrum consists of a delta function at the carrier frequency. b) In the phasor diagram, the beam is a vector defined by a unique set of quadrature amplitudes (X_1, X_2), corresponding to c) an electromagnetic wave with well-defined amplitude and phase. d) The beam noise is represented in the optical spectrum by white noise at all sideband frequencies, and e) in the phasor diagram with an uncertainty area. Each point in this area corresponds to f) a wave with a specific amplitude and phase within the respectively uncertainties ΔE and $\Delta\phi$.

this vector from the origin represents the amplitude α_0, while the angle formed with the x-axis is the phase ϕ. All these properties are shown in Fig. 2.1a)-c).

However, this description does not fully reflect the real properties of a light beam. Besides not being perfectly monochromatic, a real beam is always affected by fluctuations in both amplitude and phase, which add noise to the "perfect" beam. These noise terms usually originate from technical sources. However, even if all technical noise were eliminated, these fluctuations would not be completely removed. There is always a minimum noise level affecting the properties of an electromagnetic wave, usually referred to as quantum noise, since it arises from the interaction between the ideal beam and the vacuum fluctuations.

It is possible to linearize the complex amplitude of the electromag-

netic field in the frequency domain as [46]

$$\tilde{A}(\Omega) = \alpha_0 \delta(\Omega) + \delta\tilde{A}(\Omega) \tag{2.2}$$

where $\Omega = \omega_0 - \omega$ denotes the frequency offset from the carrier. The first term describes a delta function at $\Omega = 0$ with amplitude α_0, while the second term represents the quantum fluctuations in the sideband frequencies.

Fig. 2.1d)-f) show how these fluctuations influence the graphical representation of the field. The optical spectrum of a monochromatic light beam is now given by a peak of non-zero intensity at the carrier frequency, together with white noise distributed over the upper and lower sideband frequencies. This noise has a constant mean amplitude and uncorrelated phase terms. The total beam is therefore the sum of uncorrelated sidebands [47]. In the phasor diagram, the beam including its fluctuations is represented by a vector whose endpoint is a circular pattern, assuming equal noise in both quadratures. The radius of this circle along each direction represents the uncertainty of the beam in the corresponding quadrature. This implies that the total beam can be described as the combination of several waves with slightly different amplitudes and phases. By suppressing the technical noise, the radius of this circle is reduced until the minimum noise level imposed by quantum mechanics is reached.

2.1.2 Origin of quantum noise

In quantum mechanics, any measurable physical quantity, or observable, is associated with an operator. It is possible to link the classical variables to their corresponding quantum operators through canonical quantization. In classical optics, a single-mode monochromatic field can be modeled as a simple harmonic oscillator. Its quantization leads to the concept that light is composed of particles, called photons, of energy $\hbar\omega$, and that the field energy has only discrete allowed states, corresponding to an integer number of photons n. These energy eigenstates are described by [2]

$$\mathcal{E}_n = \left(n + \frac{1}{2}\right)\hbar\omega. \tag{2.3}$$

From Eq. 2.3, it follows that the ground state, characterized by $n = 0$, has a non-zero energy of $1/2\hbar\omega$. This quantity is known as the zero-point energy and represents the energy of the vacuum state, so called because

it is characterized by zero photons. This energy can not be removed from the system, even at zero temperature, and it represents the origin of quantum fluctuations, also called quantum or vacuum noise [2, 46].

The unavoidable presence of these quantum fluctuations affects all the properties of light and, more generally, any quantum system. A fundamental concept in quantum mechanics related to quantum noise is the Heisenberg uncertainty principle, which describes the fundamental noise relation between physical quantities.

Heisenberg uncertainty principle

The quantization of the classical electric field described by Eq. 2.1 results in [2]

$$\hat{E}(t) = \hat{a}e^{-i\omega t} + \hat{a}^\dagger e^{i\omega t} = \hat{X}\cos(\omega t) + \hat{Y}\sin(\omega t). \tag{2.4}$$

Here, $\hat{a}^\dagger$ and $\hat{a}$ are the creation and annihilation operators, which respectively increase or decrease the number of photons n in the state. Their product defines the photon number operator $\hat{n} = \hat{a}^\dagger\hat{a}$. The quadrature-phase amplitude operators $\hat{X}$ and $\hat{Y}$ are defined in terms of creation and annihilation operators as

$$\hat{X} = \hat{a} + \hat{a}^\dagger \qquad \hat{Y} = \left(\hat{a} - \hat{a}^\dagger\right)/i. \tag{2.5}$$

As in the classical case, the uncertainties of these operators define the noise of the field. Because of their non-zero commutation relation, $[\hat{X}, \hat{Y}] = 2i$, the Heisenberg uncertainty principle imposes a lower limit to the product of their uncertainties:

$$\Delta X \Delta Y \geq \left(\frac{1}{2i}\langle[\hat{X}, \hat{Y}]\rangle\right)^2 \implies \Delta X \Delta Y \geq 1. \tag{2.6}$$

This means that it is not possible to measure both quadratures simultaneously with high precision: reducing the uncertainty of one quadrature leads to an increase of the uncertainty of its conjugate.

2.2 Vacuum and coherent states

As mentioned before, the vacuum state is the lowest energy state of the electromagnetic field. It has zero mean amplitude and, therefore, it sits at the origin of the phasor diagram. By displacing the vacuum state,

a coherent state is obtained. This operation corresponds to assigning a non-zero amplitude to the field while maintaining all the noise properties unchanged.

For the vacuum and the coherent state, the two quadrature operators have equal unitary uncertainties, $\Delta X = \Delta Y = 1$, meaning that the noise is equally distributed among the quadrature amplitudes. This relation leads to the minimum value allowed by the Heisenberg uncertainty inequality in Eq. 2.6, also called zero-point fluctuation since it represents the noise of the ground state. The probability distribution of the field in the phasor diagram, which is related to the probability of measuring the two quadratures, is Gaussian. Therefore, as shown in Fig. 2.2, the vacuum state is represented by a circular distribution with unit variance centered at the origin of the plane, while the coherent state corresponds to a vacuum state displaced by a complex value α proportional to its amplitude. In both cases, the noise is phase independent. Because of these properties, a coherent state is the quantum state that best represents a classical low-noise laser beam.

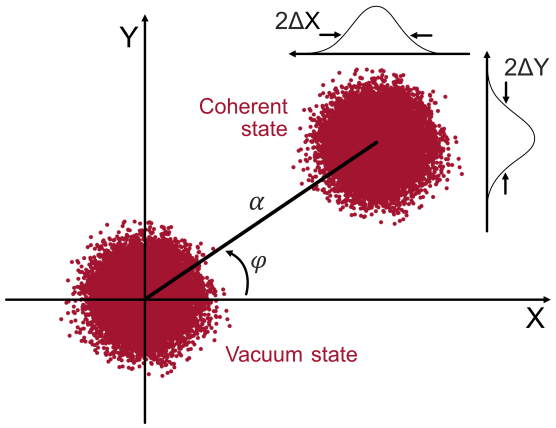

Figure 2.2: Graphical representation of a vacuum and a coherent state. Their uncertainties are defined by equal Gaussian probability distributions in both quadratures. Their noise areas correspond to the minim value defined by the uncertainty inequality.

2.3 Shot noise

Another property of a coherent state is to have a Poissonian photon number distribution. When light described by a coherent state hits a photodetector, the arrival times of the photons are random, creating a

random flux of electrons. As a consequence, the variance of the generated photocurrent reflects the intensity fluctuations of the incident light [46]. The intensity noise of a coherent state, which is equal to that of a vacuum state, is commonly referred to as shot noise in light-detection measurements. As it corresponds to the minimum quantum noise allowed by the uncertainty principle, it represents the lowest noise level achievable in a classical experiment.

The shot noise of the light detection system is described as [48]

$$V(i_{pd}) = 2qi_{pd}B = 2qRPB \tag{2.7}$$

where q is the electric charge, i_{pd} is the generated photocurrent, and B is the detection frequency bandwidth. The photodetector responsivity R is the ratio between i_{pd} and the average input optical power P. It is usually defined in terms of the photodetector quantum efficiency $\eta_D = \frac{i_{pd}\hbar\omega}{qP} = R\frac{\hbar\omega}{q}$, which is the ratio between the electron generation rate and the incident photon rate. Therefore, the shot noise level depends on the field amplitude and, moreover, it is independent of the detection frequency [46]. The shot noise is a fundamental quantity in both classical and quantum measurements, especially in the detection of squeezed states.

2.4 Squeezed states

The Heisenberg uncertainty principle sets a limit on the minimum quantum noise that two conjugate variables can have, but it does not describe how this noise is distributed between them. As shown in the previous section, the vacuum state exhibits equal uncertainty in the quadrature-phase amplitudes. A squeezed state, instead, is a particular quantum state in which the quantum noise is redistributed such that the uncertainty in one quadrature is increased while the uncertainty on the conjugate quadrature is decreased when compared to the noise of the vacuum state. The quadrature with reduced uncertainty is said to be squeezed, while the other is anti-squeezed. The product of the two uncertainties remains unchanged with respect to the vacuum state and does not go below the minimum value imposed by the uncertainty principle [4, 5].

For a squeezed state, the probability distribution of the field in the phasor diagram is no longer circular, as for the case of a coherent state. Since one quadrature has less noise than the other, the two Gaussian distributions have different widths, resulting in an elliptical noise pattern, as shown in Fig. 2.3a). The direction along which the noise is reduced

is referred to as squeezing direction, while the angle of rotation of the ellipse in the plane is the squeezing angle θ_s. A state with an arbitrary orientation is called quadrature squeezed state.

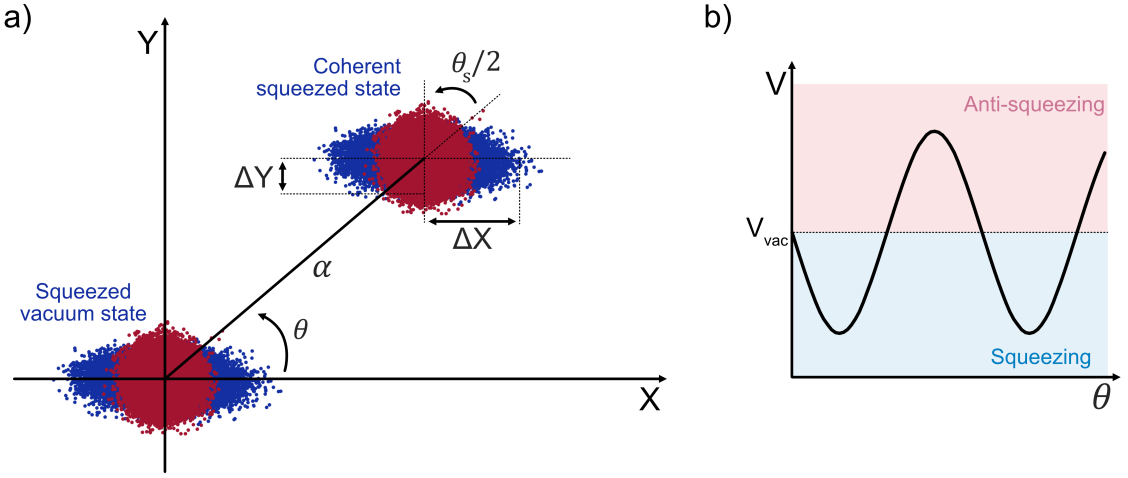

Figure 2.3: a) Graphical representation of a squeezed vacuum state and of a coherent squeezed state (blue) in comparison to a vacuum and a coherent state (red). In the first two states, the uncertainty on the Y quadrature is squeezed compared to the vacuum and the coherent states, respectively, while the uncertainty in X is stretched. b) Variance of the general quadrature $X(\theta)$ for a squeezed state. When θ equals half the squeezing angle θ_s, the variance reaches its minimum, while when they have a $\pi/2$ shift, the variance is maximum. In the former case, V falls below the constant variance of the vacuum state V_{vac}, showing squeezing, while in the latter case, $V > V_{vac}$ showing anti-squeezing.

Mathematically, a squeezed state can be described by the action of the following squeezing operator, applied to either a coherent or a vacuum state [2, 46]:

$$\hat{S}(\xi) = e^{\left(\xi \hat{a}^{\dagger 2} - \xi^* \hat{a}^2\right)/2}. \tag{2.8}$$

Here, $\xi = r_s e^{i2\theta_s}$ is the squeezing parameter, where r_s quantifies the noise reduction. The variance of the quadrature $\hat{X}(\theta) = \hat{a}e^{-i\theta} + \hat{a}^\dagger e^{i\theta}$, which is a generalization of Eq.s 2.5 by an arbitrary angle θ, is given for a squeezed state by

$$V\left(\hat{X}(\theta)\right) = \cosh(2r_s) - \sinh(2r_s)\cos(\theta - \theta_s/2). \tag{2.9}$$

As shown in Fig. 2.3b), $V\left(\hat{X}(\theta)\right)$ is a periodic function that goes below the variance of the vacuum state $V_{vac} = 1$ for specific values of θ.

In this sense, squeezed states have phase-dependent noise. This variance is precisely the quantity measured experimentally to characterize a quadrature squeezed state in a homodyne detection scheme [5,49]. Here, the squeezed light is combined with a high intensity laser beam, usually known as the local oscillator (LO). The quadrature angle θ is varied experimentally by sweeping the LO phase. The measured variance is then compared to that of the LO alone, which corresponds to the variance of a coherent state and, therefore, to the shot noise.

Fig. 2.3a) shows two possible squeezed states. The squeezed vacuum state, obtained by applying $\hat{S}(\xi)$ to the vacuum state, is centered at the origin of the phase space. In this case, the noise is squeezed along the Y quadrature and stretched along X. Although the squeezed vacuum state has zero mean amplitude like the vacuum state, its energy is higher, given by $\hbar\omega(\sinh^2(\xi) + 1/2)$ [50]. By displacing this state, a coherent squeezed state is generated. In general, a squeezed state with non zero mean amplitude is called bright squeezed state.

Fig. 2.4 provides an intuitive illustration of the time evolution of the electric field strength of some squeezed states, similarly to the classical description of an electromagnetic wave. For a coherent state (a), the expectation value of the field operator $\langle\hat{E}\rangle$ evolves as a classical sinusoidal field. The thickness of the curve represents the field fluctuations, that in this case are time independent. Fig. 2.4b) and Fig. 2.4c) show how the orientation of the noise ellipse in the phasor diagram determines the noise properties of coherent squeezed states. If the squeezing direction is aligned with the quadrature defining the field amplitude, in this case X, the state is called amplitude squeezed state (b). Here, the peaks of the electric field show minimum fluctuations. On the other hand, if the squeezing direction is orthogonal to X, the state is known as phase squeezed state (c), for which the minimum uncertainty occurs when the mean field amplitude is zero. In contrast, in a vacuum state (d), the mean field amplitude is always zero, with constant noise equal in magnitude to (a). In a squeezed vacuum state (e), instead, the noise oscillates in time following the rotation of the noise ellipse [2, 49, 51, 52].

The main property of the amplitude squeezed states is that they exhibit lower intensity fluctuations than a coherent state. Their photon number distribution is therefore sub-Poissonian, indicating a more ordered photon flux and the presence of correlations between photons [46].

In the previous section, the quantum noise of a coherent state was described as uncorrelated white noise across the upper and lower side-

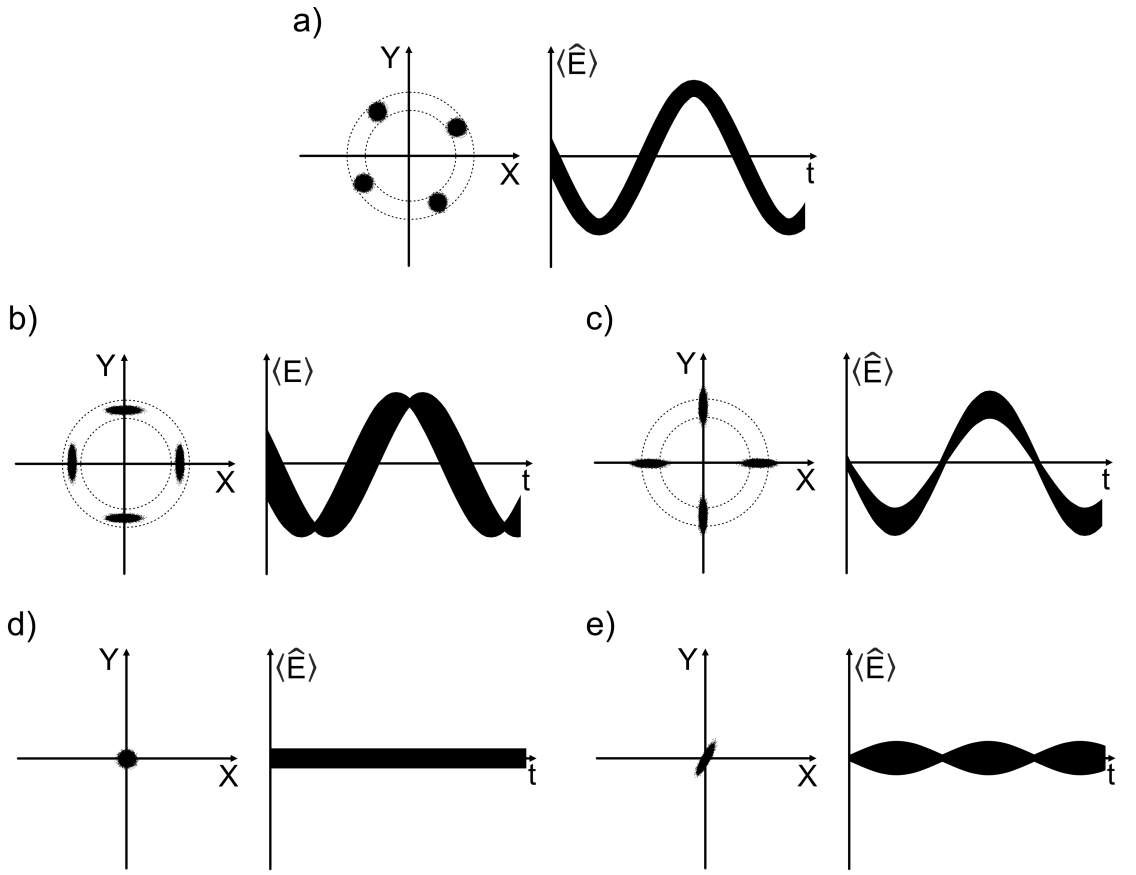

Figure 2.4: Evolution of a) a coherent state, b) an amplitude squeezed coherent state, c) a phase squeezed coherent state, d) a vacuum state, and e) a squeezed vacuum state in the phasor diagram and their respective time evolving fields.

band frequencies. In the case of a squeezed state, noise reduction can be explained by the introduction of partial correlations between noise components at symmetric sideband frequencies [46]. Such correlations are described by the second-order terms of the creation and annihilation operators in the squeezing operator defined by Eq.2.8, and can only be generated by nonlinear processes, which will be discussed in the next Chapter.

Chapter 3

Squeezed light sources

The possibility of rearranging the quantum noise in a squeezed state arises from the correlations between the fluctuations of the quadrature-phase amplitudes introduced by a nonlinear optical process. Over the years, several nonlinear materials in both bulk and integrated optics have been used for the generation of squeezing, whether in OPAs or OPOs. In this Chapter, we describe the fundamentals of squeezing generation through nonlinear processes in such devices. In particular, we focus on parametric nonlinear processes, in which optical energy is conserved, such as three-wave mixing (TWM) and four-wave mixing. Other nonlinear effects, like Raman or Brillouin scattering, in which the photons interact with the phonons in the material, are not discussed here. Moreover, the main characteristics of OPAs and OPOs in terms of squeezing generation are reviewed.

3.1 Nonlinear interactions

Nonlinear processes play a fundamental role in classical and quantum optics, as they allow for wave mixing and the generation of new frequency components. This mixing applies not only to the phases and amplitudes of the fields, but also to their fluctuations, enabling a redistribution of noise among the quadrature-phase amplitudes of a single or multiple fields. Quantum states of light, therefore, can not be generated by the manipulation of classical light through linear devices. A nonlinear process induced by an intense pump beam is required to give rise to the correlations between quantum fluctuations that form the basis of the non-classical properties of light [46].

As seen in Chapter 2, a squeezed state is described by applying the operator defined in Eq.2.8 to a coherent state or a vacuum state. This implies two things about the generation processes. First, there are two possible initial conditions for the field that is to be squeezed. One approach is to start from a classical beam with non-zero amplitude, described by a coherent state; the other is to start directly from the quantum fluctuations of the vacuum. In either case, the squeezed beam is always accompanied by a strong pump beam, which is necessary to initiate the generation process. In the latter case, the field is in a squeezed vacuum state, while in the former case it is in a bright squeezed state. Note that this terminology does not imply that the squeezed state has high power. On the contrary, bright squeezed states are usually much weaker than the input pump beam. The second concept related to the definition of the squeezing operator is that Eq.2.8 contains second-order terms of $\hat{a}$ and $\hat{a}^\dagger$ in the exponential. These terms represent the product of two fields, which can not be obtained from a linear evolution, but instead imply a nonlinear interaction [2, 5].

3.1.1 Three-wave and four-wave mixing processes

The nonlinear properties of optical materials are defined by the response of the electrons to an externally applied electric field. In practice, this response is represented by the nonlinear dielectric polarization vector $\mathbf{P}$ and its dependence on the electric field $\mathbf{E}$ of the input pump beam through the nonlinear susceptibility χ and the electric permittivity ϵ_0 [53]

$$\mathbf{P} = \epsilon_0 \left(\vec{\chi}^{(1)} \cdot \mathbf{E} + \vec{\chi}^{(2)} : \mathbf{EE} + \vec{\chi}^{(3)} \vdots \mathbf{EEE} + ... \right). \tag{3.1}$$

Here, the first-order term describes the linear response of the system, while the second- and third-order terms are responsible for nonlinear processes such as self-phase modulation (SPM), cross-phase modulation (XPM), TWM, and FWM. These processes form the basis of some of the most intriguing properties of optical materials, not only for quantum applications but also in classical photonics.

In particular, the $\chi^{(2)}$ susceptibility is responsible for TWM, which represents the interaction of three optical waves and their mutual power transfer. It is usually dominant in bulk crystal materials that lack inversion symmetry, such as lithium niobate ($LiNbO_3$) and potassium titanyl phosphate (KTP). The nonlinear process most commonly used in these $\chi^{(2)}$ materials is parametric-down conversion, in which the power

of a strong high-frequency laser beam is converted into two lower-energy beams.

On the other hand, the $\chi^{(3)}$ susceptibility is responsible for FWM, where interactions take place between four optical waves. Its strength is usually weaker than its second-order counterpart, and therefore is mainly exploited in media in which $\chi^{(2)}$ is zero, such as silica (SiO_2) and silicon nitride (SiN). In these materials, $\chi^{(3)}$ is also responsible for the Kerr nonlinear effect, namely the dependence of the refractive index n on the intensity of the applied field $|E|^2$

$$n = n_0 + n_2|E|^2, \tag{3.2}$$

with n_0 being the constant refractive index of the medium and n_2 the nonlinear coefficient proportional to $\chi^{(3)}$. Since the phase of a wave depends on the refractive index of the medium, the Kerr nonlinear effect causes an intensity-dependent phase shift. As shown in Fig. 3.1, the regions with higher amplitude are associated with an increased phase shift as a direct consequence of the nonlinear refractive index, causing a distortion of the noise circle. This phenomenon is used mainly in optical fibers for the squeezing of coherent states [54–56], in which weak nonlinearity is compensated for by a long interaction time.

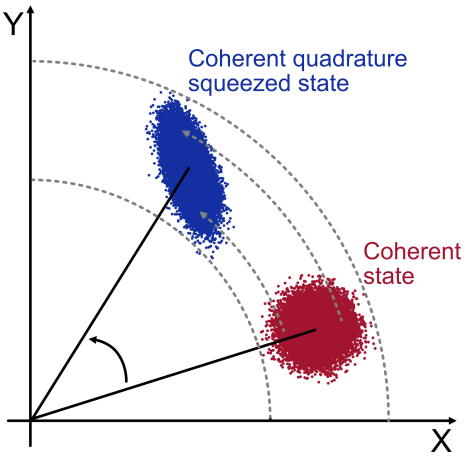

Figure 3.1: Graphical representation in the phasor diagram of the creation of a coherent quadrature squeezed states through the Kerr nonlinear effect acting on a coherent state. The gray arrows show the changes on the phase fluctuations depending on the initial intensity fluctuations.

Fig. 3.2 shows a schematic of the most commonly used TWM and FWM parametric processes for squeezing generation. Together with the

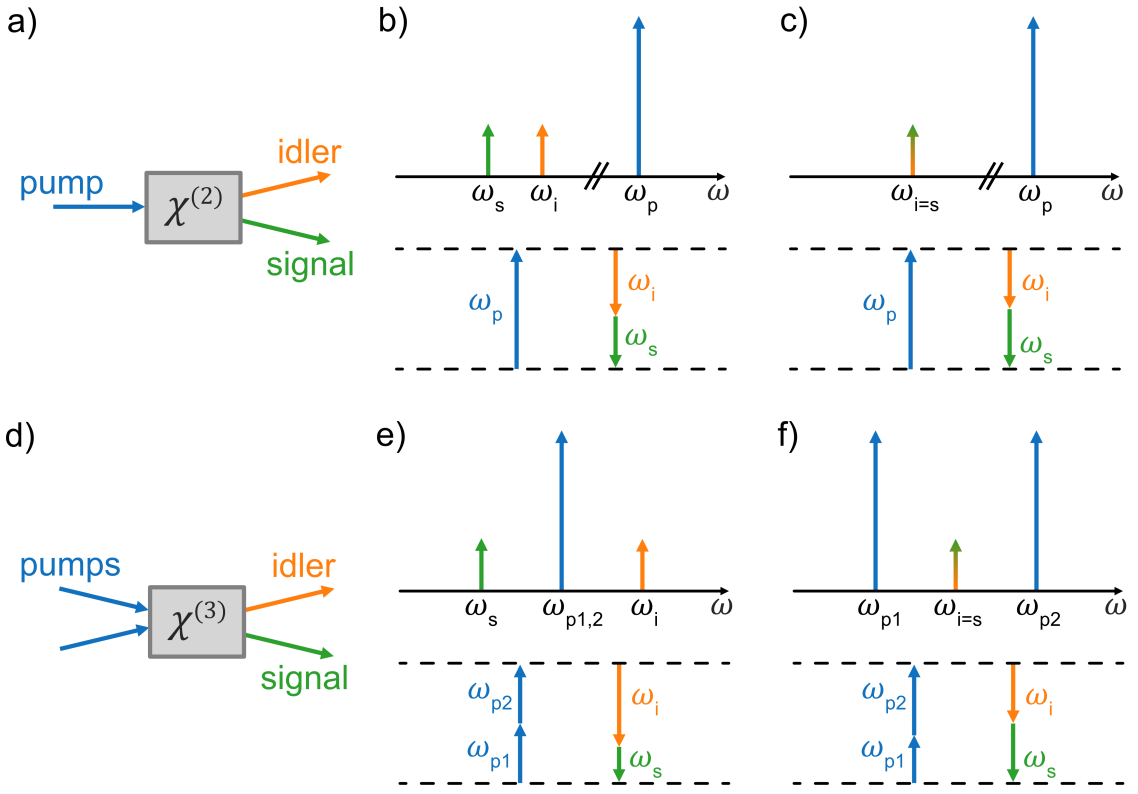

Figure 3.2: Schematics of the a) $\chi^{(2)}$ and d) $\chi^{(3)}$ nonlinear processes. The frequency distribution in the optical spectrum and between virtual energy levels is shown for: b) non-degenerate TWM, c) degenerate TWM (PDC), e) single pump non-degenerate FWM, f) dual pump degenerate FWM.

input pumps, the other two fields involved in both processes are usually referred to as signal and idler, and they are the fields that exhibit squeezing properties. The parametric nature of these processes ensures energy conservation among the interacting fields. Defining the pump, signal and idler fields with angular frequencies ω_p, ω_s and ω_i, respectively, energy conservation in the TWM process is expressed as $\omega_p = \omega_s + \omega_i$, while for the FWM process it reads $\omega_{p1} + \omega_{p2} = \omega_s + \omega_i$.

In addition to energy conservation, momentum conservation is also needed. Each field acquires a certain phase ϕ while propagating in a medium. The phase-matching condition for the TWM and FWM processes are, respectively, $\phi_p = \phi_s + \phi_i$ and $\phi_{p1} + \phi_{p2} = \phi_s + \phi_i$. The acquired phase in a nonlinear dispersive medium is usually described in terms of the frequency dependent propagation constant $\beta(\omega)$. In this case, the phase-matching condition $\Delta\beta_L + \Delta\beta_{NL} = 0$ describes the balance between the linear phase accumulated by each wave and the additional

contribution due to nonlinear processes [53]. This balance determines both the occurance and the efficiency of TWM and FWM processes. It is therefore important to engineer the device used for squeezing generation in order to satisfy the phase-matching condition.

3.1.2 Interaction Hamiltonian

The interaction Hamiltonian describing all nonlinear wave mixing processes, including SPM, XPM, TWM, and FWM, is derived directly from the nonlinear polarization operator $\hat{P}^{NL}$, obtained from the quantization of the nonlinear terms of Eq.3.1 [2]:

$$\hat{H}_{int} = \frac{1}{2}\int \hat{P}^{NL}(\mathbf{r},t)\cdot\hat{E}(\mathbf{r},t)d^3\mathbf{r}. \tag{3.3}$$

The TWM term in Eq.3.3 is given by

$$\hat{H}_{TWM} = i\hbar\eta\hat{a}_1^\dagger\hat{a}_2^\dagger\hat{a}_3 + h.c., \tag{3.4}$$

which describes the interaction of three waves represented by the operators $\hat{a}_1$, $\hat{a}_2$ and $\hat{a}_3$. Here, *h.c.* denotes the Hermitian conjugate, and η is proportional to the nonlinear susceptibility of the material. Following the same procedure, the interaction Hamiltonian of the FWM process is

$$\hat{H}_{FWM} = i\hbar\eta\hat{a}_1^\dagger\hat{a}_2^\dagger\hat{a}_3\hat{a}_4 + h.c.. \tag{3.5}$$

Usually, the material nonlinearity is relatively small and, therefore, a necessary condition for nonlinear processes to occur is that one of the three fields involved in TWM, and two fields in FWM, are sufficiently strong to be modeled as classical fields with complex amplitude A. Defining $\zeta = \eta A_3$ for TWM and $\zeta = \eta A_3 A_4$ for FWM, Eq.s 3.4-3.5 become

$$\hat{H}_{2p} = i\hbar(\zeta\hat{a}_1^\dagger\hat{a}_2^\dagger - \zeta^*\hat{a}_1\hat{a}_2). \tag{3.6}$$

The system described by Eq.3.6 evolves according to the unitary operator

$$\hat{U} = e^{-i\hat{H}_{int}^P t/\hbar} = e^{(\varrho\hat{a}_1^\dagger\hat{a}_2^\dagger - \varrho^*\hat{a}_1\hat{a}_2)/2}, \tag{3.7}$$

with $\varrho = 2t\zeta$. Eq.3.7 has exactly the same structure as the squeezing operator in Eq.2.8, showing that a parametric nonlinear interaction can result in the generation of squeezed states. The key requirement is that the Hamiltonian is at least quadratic in the creation and annihilation operators [50].

The processes described by this Hamiltonian are usually referred to as two-photon processes, since they involve the simultaneous creation of two photons in the signal and idler fields and the annihilation of one or two photons of the pump field(s).

3.2 Effect of losses on squeezed light

So far, we have discussed the definition of squeezed states and their generation in the ideal case, i.e. assuming no losses in the system. However, a real device is always characterized by internal and coupling losses which, in general, represent the main limiting factors for the possible generated squeezed level. We discuss this dependence for specific squeezed states in more detail in Chapter 4, while here we focus on the effect of measurement loss on the detected squeezing.

We saw that to quantify the noise reduction in a general quadrature squeezed state one should look at its variance, defined by Eq.2.9, and compare it with the shot noise level. However, what can be measured in a real experiment is the variance of the squeezed state affected by the losses intrinsic of any experimental setup. In most cases, these losses can be measured in order to retrieve the actual value of squeezing generated at the source. The dominant loss contributions usually arise from the light propagation through multiple optical components and from the detection apparatus.

Conventionally, the effect of the total setup loss on the fluctuations of the quadrature operator $\hat{X}(\theta)$ is modeled by a beam splitter, which is used to describe the linear interaction between two fields. In this case, the beam splitter has the transmission coefficient equal to the square root of the setup efficiency $\sqrt{\eta}$, which has squeezed light in one input port and vacuum fluctuations in the other, as shown in Fig. 3.3. The corresponding relation is [46]

$$\Delta\hat{X}(\theta)_{out} = \sqrt{\eta}\Delta\hat{X}(\theta)_{in} + \sqrt{1-\eta}\Delta\hat{X}(\theta)_{vac}. \tag{3.8}$$

The variance of the measured output quadrature is then

$$V_{\text{out}} = \eta V_{\text{in}} + (1-\eta)V_{\text{vac}}, \tag{3.9}$$

where the variance of the vacuum state is $V_{\text{vac}} = 1$ by definition.

From an experimental point of view, any loss is detrimental to the final squeezing level that can be measured. These losses lead to an increase of the total noise of the state, effectively transforming the squeezed

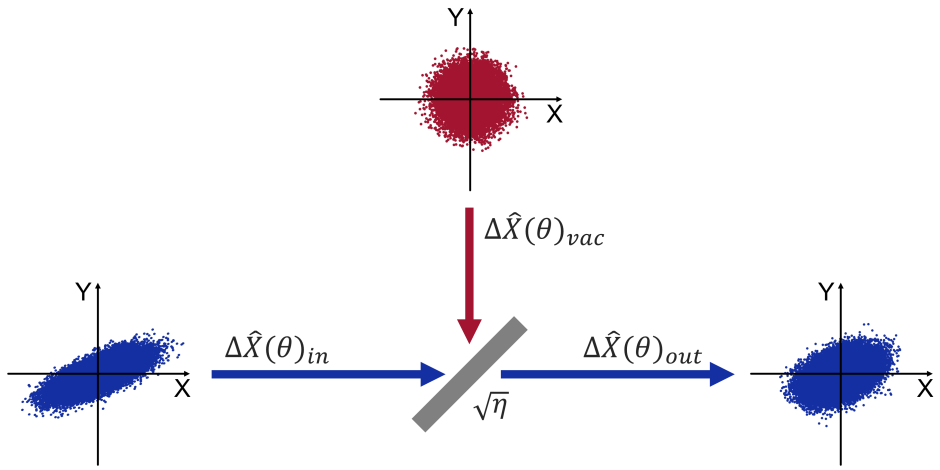

Figure 3.3: Beam splitter model of the effect of losses on the quadrature fluctuations in the phasor diagram.

noise ellipse into the noise circle of a coherent state. It is therefore crucial to minimize all sources of loss in the setup, both during the squeezing generation and in subsequent applications.

3.3 Squeezing generation in OPAs and OPOs

The typical devices used for squeezing generation are OPAs and OPOs [57]. In general, both devices rely on a nonlinear material that enables the amplification or generation of new frequency components.

In bulk optics, typical OPAs are based on nonlinear crystals [16, 58–60], most of which exploit the $\chi^{(2)}$ susceptibility, or on highly nonlinear optical fibers [61–63], which rely on the $\chi^{(3)}$ susceptibility of silica. One of the first demonstrations of squeezing generation was achieved using the Kerr nonlinearity in optical fibers [64]. However, it is now known that other nonlinear processes, like Brillouin and Raman scattering, limit the achievable squeezing level in these systems [55, 65]. In integrated devices, instead, a typical OPA consists of a long high-confinement waveguide in which the nonlinearity builds up as light propagates through it. In this case, the typical platform for squeezing generation is thin film LiNbO3 [34, 36, 66], where quasi phase-matching is reached by periodic polling.

In typical OPAs, the efficient generation of high levels of squeezing requires very high levels of pump power, which are often difficult to reach with continuous-wave (CW) lasers. As a result, pulsed pumps are often used in OPA-based squeezers. In these devices, squeezing ex-

hibits a broad frequency bandwidth (of the order of THz), limited only by the phase-matching condition of the medium, which defines the parametric gain spectrum. As shown in Fig. 3.4a), in the case of squeezed vacuum, the entire spectrum of vacuum fluctuations within the parametric gain bandwidth is amplified and squeezed. In addition to their use as squeezers, OPAs have also been employed in recent demonstrations for the measurement of squeezing. Phase-sensitive OPAs can amplify the squeezed quadratures without adding extra noise, enabling direct optical power detection. This amplification also makes squeezing measurements more tolerant to losses and low detection efficiencies [67–69].

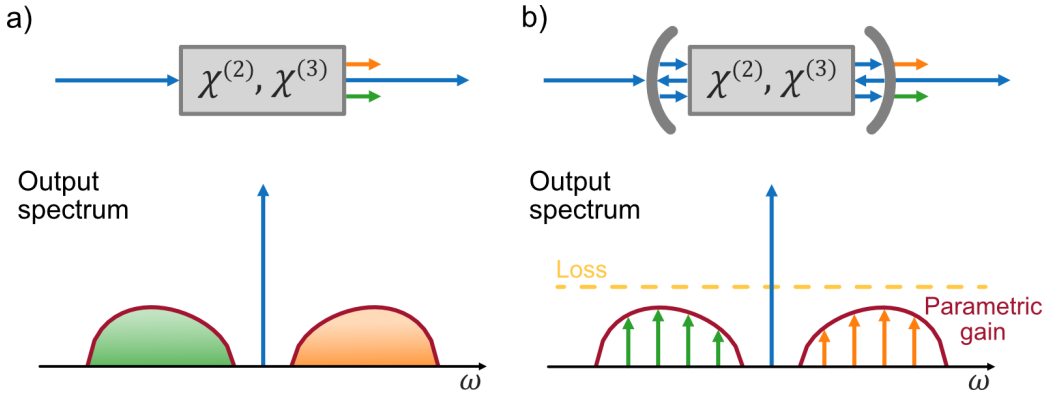

Figure 3.4: a) The TWM or FWM processes in an OPA occurs while light travels through the nonlinear material. The amplification and squeezing of the vacuum fluctuations is continuous within the broad parametric gain spectrum defined by the phase-matching condition, shown here for a FWM process. b) In an OPO, the nonlinear material is placed inside an optical cavity. The resulting spectrum is characterized by the cavity resonances, which define the narrow squeezing bandwidth and discrete signal and idler positions.

In OPOs, instead, the nonlinear medium is placed inside an optical cavity to enhance the nonlinear interactions among the optical fields, as shown in Fig. 3.4b). This solution efficiently amplifies the vacuum fluctuations or weak signals and leads to an efficient generation of squeezing. All OPOs are characterized by a parametric threshold, which corresponds to the minimum pump power required for the parametric gain to overcome cavity losses and initiate the oscillations at new frequencies. In classical optics, these devices are typically pumped above threshold to generate observable output power. In quantum optics, however, and in particular to generate squeezed vacuum states, OPOs are usually pumped just below threshold, where infinite squeezing is expected in the ideal case of a lossless device [2, 70]. In this condition, the nonlinear

process is usually referred to as spontaneous FWM, since only vacuum fluctuations are involved in the process.

In these OPOs, very high pump powers are not required, allowing the operations with CW lasers. However, the squeezing spectrum is limited by the longitudinal resonant modes of the cavity. Therefore, the squeezing bandwidth is restricted to the cavity resonance linewidth (typically up to GHz), and the signal and idler frequencies are limited to the cavity resonance frequencies. Nowadays, the highest measured squeezing level is 15 dB, achieved with a periodically poled KTP crystal in a double resonant cavity [18]. In bulk optics, these cavities can become very large and unstable against phase noise. Therefore, the interest of the community in the last decade has shifted toward their miniaturization. This interest has also been pushed by the recent advances in the fabrication of integrated photonic devices and by improved understanding of their behavior in classical optics [33]. In the case of integrated OPOs, the most widely used devices are microring resonators based on SiN [38–40, 42, 71], in which the FWM arising from $\chi^{(3)}$ susceptibility is the dominant process. Some state-of-the-art generations of different relevant squeezed states based on these devices are discussed in the next Chapter, along with examples of their applications.

Chapter 4

Overview of some squeezed states and their applications

In this Chapter, we present some of the most commonly used types of vacuum and bright squeezed states that can be generated from the nonlinear processes discussed previously. More attention is paid to OPO devices, especially in PICs, since the squeezed states examined in this thesis arise from the third-order nonlinearity of SiN-based integrated microring resonators.

In general, a complete description of the properties of a squeezed state is given by the squeezing spectrum, which is derived from the specific quantum model of the generating system. For a detailed analysis, the quantum model should be as complete as possible, taking into account all the possible effects of the linear and nonlinear propagation of the light in the medium, with particular attention on all types of intrinsic losses in the device.

The common way to obtain the squeezing spectrum in the quantum formalism is to start from the complete Hamiltonian of the system, which includes the linear propagation of the m modes involved in the process and the term for the interaction processes described by Eq. 3.3 [1, 2, 50, 72]. The total Hamiltonian is then used to calculate the Heisenberg equations of motion of the mode operators. Solving these coupled equations, together with the appropriate input-output relations, gives the time evolution of the creation $\hat{a}_m^\dagger(t)$ and annihilation $\hat{a}_m(t)$ operators of the output squeezed fields, which are transformed in the

Fourier domain according to

$$\tilde{a}_m^{(\dagger)}(\Omega) = \frac{1}{\sqrt{2\pi}} \int \hat{a}_m^{(\dagger)}(t) e^{i\Omega t} dt. \tag{4.1}$$

These operators are usually used to define the generic quadrature operator $\tilde{X}_\varphi(\Omega)$, whose specific form depends on the system and the type of squeezing under investigation. Finally, the variance V_{sq} of this operator defines the squeezing spectrum as [2]

$$S_{X_\varphi}(\Omega) = \frac{V_{sq}}{V_{vac}} = \frac{\langle |\tilde{X}_\varphi(\Omega)|^2 \rangle}{\langle |\tilde{X}_\varphi^0(\Omega)|^2 \rangle}, \tag{4.2}$$

here normalized by the variance V_{vac} of the vacuum quadrature operator $\tilde{X}_\varphi^0(\Omega)$. In practice, Eq.4.2 represents the noise spectrum of the squeezed light, that is, the noise power as a function of the detection frequency offset Ω from the carrier frequency ω_m of the squeezed modes [46]. It is usually evaluated experimentally with a balanced photodetector and a spectrum analyzer.

In the following sections, for each state, we qualitatively discuss the properties of the corresponding squeezing spectrum, focusing on the main limiting factors for reaching high squeezing levels in state-of-the-art integrated sources. More attention is paid in describing the intensity difference squeezing measured in Paper A and the two-mode quadrature squeezing analyzed in Paper B. Finally, we describe state-of-the-art examples of their applications in quantum information processing.

4.1 Vacuum squeezing

4.1.1 Two-mode quadrature vacuum squeezing

A two-mode quadrature vacuum squeezed state describes a state formed by two distinct fields, the signal and the idler, whose quadrature fluctuations are correlated by a nonlinear process. In the following, we use the formalism for which the two modes are defined by distinct frequencies, with $m = s, i$ and $\omega_s \neq \omega_i$. For this reason, the nonlinear processes used to generate two-mode quadrature squeezing require the creation of two distinct frequency modes. Therefore, the relevant processes, among those described in Fig. 3.2, are the non-degenerate TWM, and the single pump non-degenerate FWM, shown in Fig. 4.1a). In both cases, the initial signal and idler fields are assumed to be in a vacuum state.

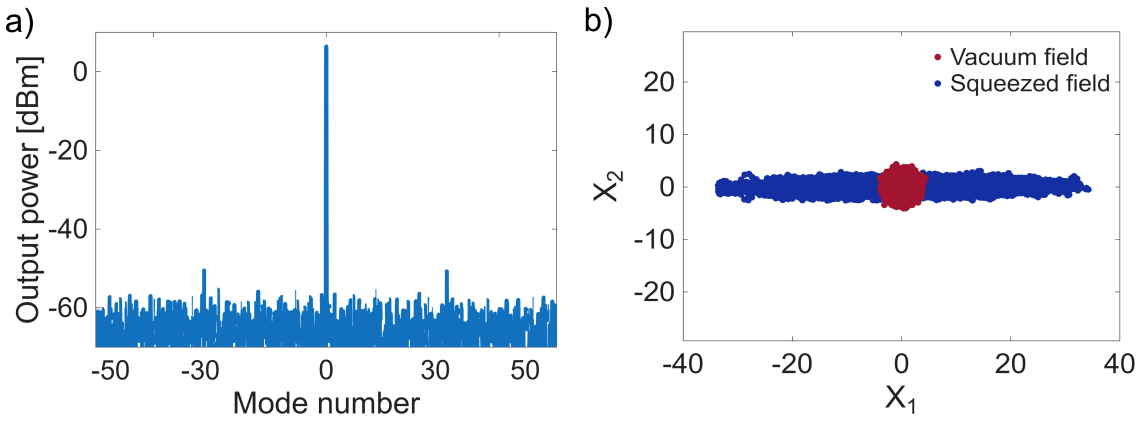

Figure 4.1: Sem-classical simulation of a two-mode squeezed state. a) Optical spectrum of the spontaneous FWM process. b) Phasor diagram showing perfect squeezing in X_2 and anti-squeezing in X_1. The noise in the latter quadrature is amplified by the propagation loss included in the simulation.

The squeezing operator for this state is defined as [2]

$$\hat{S}(\xi) = e^{\left(\xi \hat{a}_s^\dagger \hat{a}_i^\dagger - \xi^* \hat{a}_s \hat{a}_i\right)/2}, \tag{4.3}$$

where $\hat{a}_{s,i}^\dagger$ and $\hat{a}_{s,i}$ are the creation and annihilation operators of the signal and idler modes. In this case, two-mode quadrature squeezing is a shared property of the two modes. In other words, it is the sub-system composed of the paired modes that is in a squeezed state [5, 73]. If we analyze the quadratures of the two individual modes separately, we would not measure any squeezing. It is necessary to combine the in-phase and quadrature components of the two fields in order to properly analyze the two-mode quadrature squeezing. For this reason, we introduce the collective creation and annihilation operators of the combined fields [1]

$$\hat{b} = \frac{1}{\sqrt{2}} \left(\hat{a}_s + \hat{a}_i\right); \tag{4.4}$$

$$\hat{b}^\dagger = \frac{1}{\sqrt{2}} \left(\hat{a}_s^\dagger + \hat{a}_i^\dagger\right). \tag{4.5}$$

The resulting two-mode quadrature operator of the signal and idler sub-system has the form

$$\hat{X}_\varphi = \frac{1}{2} \left(\hat{b} e^{-i\varphi} + \hat{b}^\dagger e^{i\varphi}\right), \tag{4.6}$$

with φ describing the angle of the squeezing direction in the phasor diagram. A typical representation of a two-mode quadrature vacuum

squeezed states is shown in Fig. 4.1b), in which $\hat{X}_1 = \hat{X}_{\varphi=0}$ and $\hat{X}_2 = \hat{X}_{\varphi=\frac{\pi}{2}}$. Here, the squeezing angle φ is optimized to have perfect squeezing along X_2 and anti-squeezing along X_1.

In the specific case of squeezing from an OPO, the analysis of the squeezing spectrum derived from Eq.4.2 shows that the squeezing level depends on several intrinsic parameters of the device [2,50,70]. In particular, two main limiting factors are the intrinsic propagation loss and the loss in the coupling to and from the cavity, described by the coefficients κ_i and κ_c, respectively. The maximum achievable squeezing level also depends on the ratio between the input pump power P_{in} and the parametric oscillation threshold P_{th}. In addition, it is important to note that in these devices, the pump, signal, and idler beams can oscillate only at frequencies in proximity to the longitudinal modes allowed to exist inside the cavity. We define the detuning from the cavity frequencies $\omega_{s,i}^{cav}$ for the signal and idler modes as $\Delta_{s,i} = \omega_{s,i} - \omega_{s,i}^{cav}$. This detuning depends on several factors, such as the input pump laser detuning from the cavity mode and the device dispersion. The effects of these parameters on the squeezing spectrum are discussed in more detail in the following paragraphs.

In the case of a lossless device, the two-mode squeezing spectrum is shown in Fig. 4.2a), normalized such that $S_{X_\theta} = 1$ represents the noise spectrum of the vacuum state. The noise suppression reaches its maximum ($S_{X_\theta} = 0$) when the device is pumped at threshold $P_{in} = P_{th}$ and when the signal and idler are in resonance ($\Delta = 0$); it decreases as

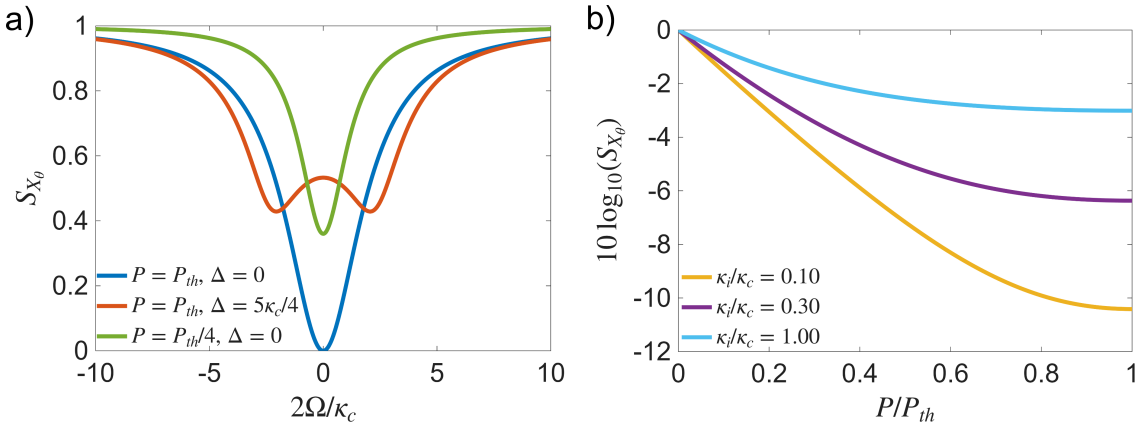

Figure 4.2: a) Two-mode quadrature squeezing spectrum of a generic lossless OPO for three combinations of resonance detuning Δ and below threshold pump power P. b) Dependence of the squeezing level on the coupling condition κ_i/κ_c and on P, assuming signal and idler at resonance ($\Delta = 0$).

the pump power is reduced and as the detuning increases. Moreover, the shape of the inverted Lorentzian depends on the detuning $\Delta_{s,i}$, emphasizing that the squeezing level at the output of a cavity is frequency dependent [1].

Fig. 4.2b), instead, takes into account the effect of the losses. It shows that the squeezing is maximized by pumping the device below threshold, and when $\kappa_i \ll \kappa_c$. In this coupling regime, usually called of strong overcoupling, light escapes from the cavity faster than it is lost due to intrinsic loss, allowing the majority of the squeezed photons to be collected at the output. This dependence can be explained by the fact that squeezing arises from a two-photon process: the loss of a photon of the pair leaves the remaining one as an uncorrelated photon, causing an imbalance in the system which is translated to a reduction of the squeezing and an increase of the anti-squeezing level. The loss of both photons certainly reduces the level and the efficiency of the squeezing generation [2].

An example of an integrated OPO used for the generation of two-mode quadrature squeezing is a SiN microring resonator operated below threshold with a single pump beam [38, 44]. In this case, the squeezing measurement is conducted via homodyne detection using a bichromatic LO, whose frequencies coincide with those of the signal and idler modes, and that must be phase coherent with the measured signals to suppress the system technical noise. The generation of three phase coherent beams (two LO components and the input pump) is therefore a strong limiting factor affecting the quality of the measurement. One direct solution is to phase-lock three separate lasers [38]. The alternative solution proposed in Ref. [44], instead, is based on a simplified setup that requires only one input laser to generate both the vacuum squeezed paired modes and the LO. The latter is based on a classical electro-optic (EO) comb in which the spacing and the central frequency are tuned such that two comb lines, then filtered with a wave shaper, overlap with the signal and idler modes. This technique allowed for the first demonstration in an integrated microresonator of a squeezed frequency comb made of 40 modes, showing direct measurement of a maximum 1.6 dB of quadrature squeezing. Note here that the number of modes analyzed is limited by the EO comb bandwidth and not by the squeezer.

4.1.2 Single-mode quadrature vacuum squeezing

Single-mode quadrature vacuum squeezing occurs when the signal and idler fields are degenerate, i.e., $\hat{a}_s = \hat{a}_i$. Therefore, it can be generated either by dual pump FWM or by degenerate TWM, most commonly known as spontaneous PDC, since the process occurs without an input seed. The squeezing and quadrature operators for a single-mode squeezed state were introduced in Chapter 2 to discuss the general concept of squeezing. Moreover, in the case of being generated by an OPO, the main properties of this squeezed state correspond to those of the analogous two-mode state presented above. The maximum squeezing is obtained by pumping a strongly overcoupled device just below threshold [1, 2, 46, 50].

In the case of an integrated OPO, the typical source is a SiN microresonator where two pumps of equal intensity are applied to two separate resonances to generate squeezing in the mode at the center. However, in this configuration, the achievable level of squeezing is strongly reduced by unwanted nonlinear effects, especially single-pump FWM [74]. Therefore, to ensure high-quality squeezing, it is important to engineer the devices to suppress these processes. One solution is to induce mode-spitting in the resonances involved in the extra processes, effectively removing the condition for the processes to occur, as shown in Fig. 4.3. Mode-splitting can be created using engineered devices such as photonic molecules [39, 75] or crystals [71], where the position and efficiency of the splitting are controlled by adjusting the dimension of the auxiliary ring and of the corrugations typical of the two devices, respectively.

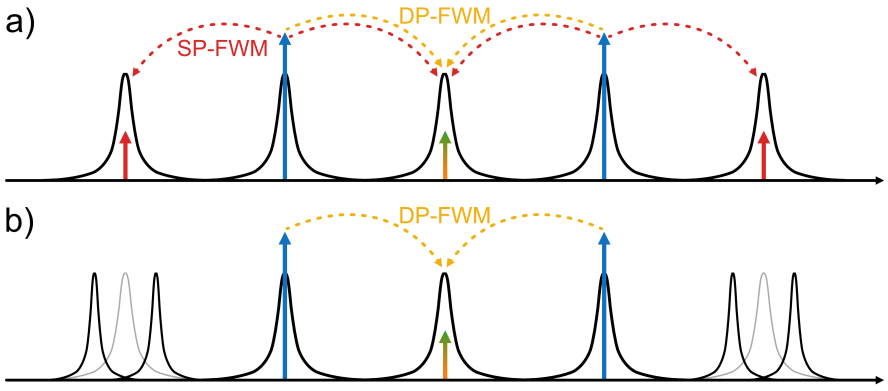

Figure 4.3: Schematic of the FWM processes in a) a classical microring resonator and b) in a device engineered to split the resonance involved in unwanted nonlinear processes. SP-FWM: single-pump FWM; DP-FWM: dual-pump FWM.

On the other hand, typical integrated OPAs employed for the generation of broadband single-mode squeezed states are high-confinement LiN waveguides [34, 36, 66]. In this case, the squeezing spectrum depends on the length of the nonlinear waveguide and on the input pump power [34]. The challenges in fabricating good-quality long periodically-polled waveguides and the limitations on the sustainable input power reduce the squeezing levels obtained from these devices. Nonetheless, a main advantage of this technique is the use of the same input laser to generate both the pump, through second harmonic generation, and the LO employed in the homodyne measurement, ensuring mutual coherence and extra noise suppression.

4.1.3 Squeezed quantum combs

One of the fundamental uses in the classical regime of third-order nonlinear integrated OPOs driven above the parametric threshold is to generate frequency combs, also called microcombs. Those are characterized by equally spaced coherent frequency modes with unique classical properties [76, 77]. Recently, the quantum nature of these microcombs has also been investigated [78, 79]. For example, Ref. [80] predicts the generation of squeezing in the modes below threshold of a soliton crystal,

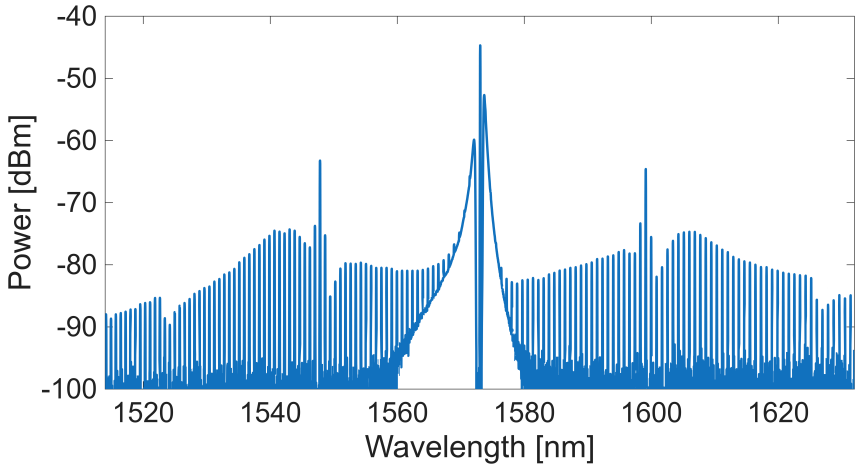

Figure 4.4: Measurement of the optical spectrum of a microcomb generated by a SiN microring resonator pumped below the parametric threshold. The central input pump is attenuated to resolve the weak comb lines in the background noise of a typical optical spectrum analyzer. Modes at wavelengths 1548 nm and 1600 nm correspond to the peak of the parametric gain and are the first to oscillate in case the device is pumped above threshold.

foreseeing the creation of a hybrid microcomb with both classical and quantum properties. Additionally, it is possible to create a full quantum microcomb by operating the microresonators below the threshold. In the previous section, the two-mode quadrature squeezed state was defined between a pair of signal and idler modes. However, the spontaneous FWM process in an OPO allows for the simultaneous generation of several quantum mode pairs, all showing two-mode quadrature squeezing, thereby creating a squeezed quantum microcomb [40, 43, 44]. Fig. 4.4 shows an example of a measurement of comb lines resulting from pumping a SiN microring resonator below the threshold, and that could potentially display quantum properties.

4.2 Bright squeezing

4.2.1 Coherent quadrature squeezing

A coherent squeezed state is a displaced single-mode or two-mode quadrature squeezed state with non-zero amplitude. It can be obtained by combining in a beam splitter a quadrature squeezed vacuum state with a coherent state, like a classical laser beam, as shown in the schematic of Fig. 4.5. Equivalently, it can also be generated by the SPM and Kerr nonlinear effect of the strong coherent pump used as input in a squeezer [81]. In this case, the coherent mode is directly converted into the squeezed mode, naturally creating a coherent squeezed state and removing the necessity of mixing two separate modes with extra components.

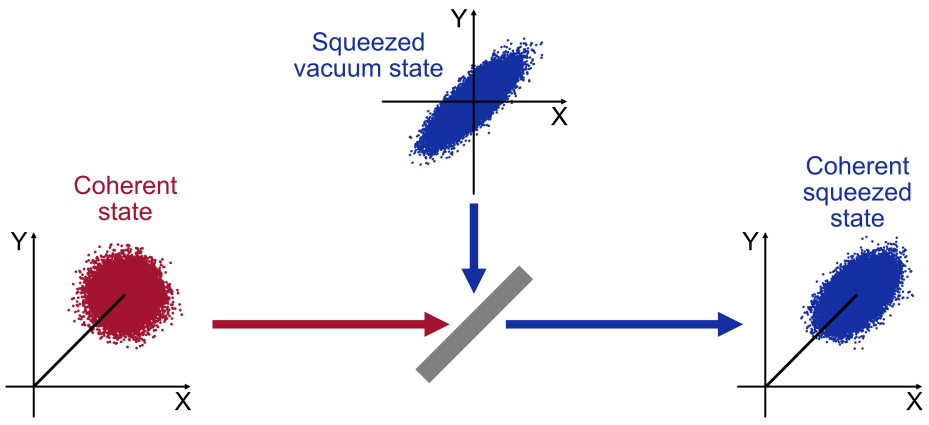

Figure 4.5: Schematic of the creation of a coherent squeezed state from the interaction in a beam splitter of a coherent state and a squeezed vacuum state.

4.2.2 Intensity difference squeezing

Intensity difference squeezing occurs between bright fields. In fact, as suggested by the name, the squeezed properties appear in the photon number difference of two distinct fields with non-zero amplitude, usually generated through single pump non-degenerate FWM in an OPO operated above threshold. Fig. 4.6a) shows an example of the three involved modes. As we can see, the signal and the idler are weaker than the input pump, but they have a sufficiently large amplitude to be displaced from the center of the phasor diagram and be directly measured in a photodetector.

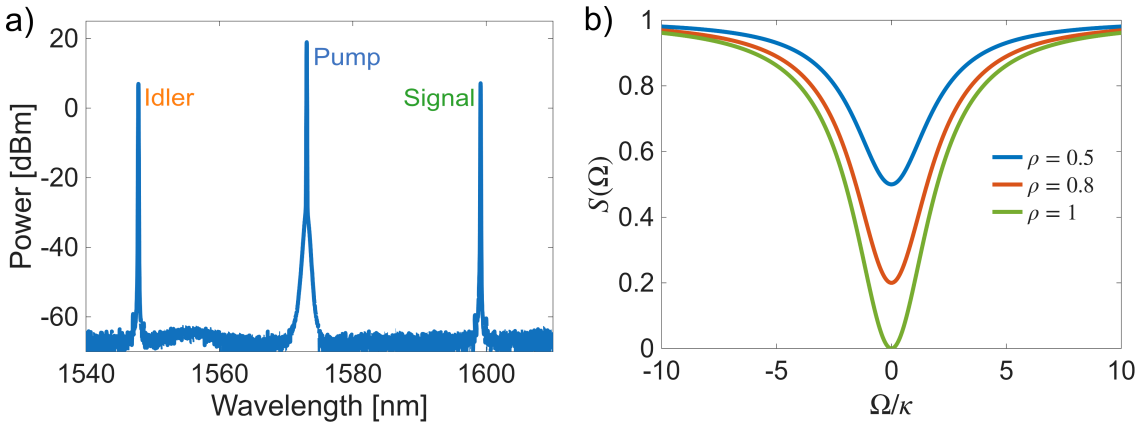

Figure 4.6: a) Measurement of the optical spectrum of the generated bright signal and idler beams. b) Spectrum of an intensity difference squeezed state generated in an OPO for three values of ρ.

Due to the energy conservation imposed by the two-photon parametric process, the signal and idler modes have the same amplitude and, therefore, the same average photon number. For this reason, they are commonly called twin beams. To analyze the intensity difference squeezing spectrum, we need to introduce the photon number difference operator, defined in terms of the signal and idler photon number operators $\hat{n}_s$ and $\hat{n}_i$ as

$$\hat{n}_\Delta = \hat{n}_s - \hat{n}_i = \hat{a}_s^\dagger \hat{a}_s - \hat{a}_i^\dagger \hat{a}_i. \tag{4.7}$$

This operator commutes with $\hat{H}_{FWM}$ when only a pair of twin beams is generated. In this case, the exact number of photons is conserved, not only its average.

In the case of a lossy OPO, the spectrum of the intensity difference

squeezing is [70]

$$S(\Omega) = 1 - \rho \frac{4\kappa^2}{\Omega^2 + 4\kappa^2} \tag{4.8}$$

in which $\kappa = \kappa_i + \kappa_c$ and $\rho = \frac{\kappa_c}{\kappa}$. Fig. 4.6b) shows $S(\Omega)$ for some combinations of parameters. As for the previous cases, the squeezing level reaches its maximum at resonance and in the strongly overcoupled regime, when $\rho \to 1$. At low offset frequencies, the squeezing level tends to the value $1 - \rho$, meaning that the achievable squeezing depends on the quality of the devices in terms of intrinsic and coupling losses. In contrast to vacuum quadrature squeezing, intensity difference squeezing is independent of the input pump power, as long as it is above the parametric threshold but still sufficiently low to not initiate cascade FWM and the oscillations of the other modes. In this case, the presence of multiple pumps, and therefore of different sources of photons, eliminates the correlations between the paired beams.

Intensity difference squeezing is the first type of squeezing demonstrated in SiN microring resonators [37], where 1.7 dB of squeezing was directly measured. In a more recent experiment [42], the level of measured squeezing has been increased to 3.5 dB by reducing the total detection loss and by using a strongly overcoupled device, which generates an inferred on-chip squeezing of 10.2 dB. In these integrated OPOs, the limiting aspects are in the fabrication procedures for achieving low intrinsic loss and a high coupling coefficient. Other similar works are described in Ref. [82, 83]. The results presented in Paper A refer to the analysis of intensity difference squeezing generated from a special engineered SiN microring resonator optimized to have strongly overcoupled resonances. In our experiment, the generation of the twin beams and their characterization follow the procedure used in these first demonstrations, also described in the Appendices.

Very recently, a new technique based on seed-assisted parametric amplification of squeezing, suggested in Ref. [43], allowed for the direct detection of 5.6 dB of squeezing, surpassing all previous measurements from integrated OPOs. Here, a seed signal, together with the generated idler, amplifies two-mode quadrature squeezed vacuum modes generated by pumping the device below threshold. The amplification is done directly in the same microring resonator used as a squeezer, effectively creating a bright squeezed state that can be analyzed without a LO. The drawback of this technique is that only the amplitude quadrature becomes accessible for measurements, transforming the analysis of quadrature squeezing

into an investigation of intensity difference squeezing.

4.3 Applications

Due to the high quality of squeezing generation reached over the years, there are several fields of application where squeezed states are nowadays employed, going from quantum computing, quantum communication and networking, to quantum sensing and metrology.

4.3.1 Photonic quantum computing

In recent years, photonic platforms have been used to demonstrate important steps toward the realization of operating quantum computers. In this context, squeezed states can be used to encode quantum information in continuous variable (CV) protocols, which exploit the continuous properties of light, such as the quadratures of the fields.

Squeezed states have been employed directly in several architectures, mainly to verify quantum computational advantage, that is, the speed-up of operations in a quantum hardware compared to a classical computer [28, 84–86]. These demonstrations are based on Gaussian boson sampling (GBS) [87], where several single-mode vacuum quadrature squeezed modes are injected into a linear interferometer composed of a large number of beam splitters, and the resulting output pattern is sampled with photon number resolving detectors. The latters require the use of vacuum squeezing to avoid saturation caused by strong bright light [88]. In 2020, GBS was implemented in a bulk setup based on $\chi^{(2)}$ photonic crystals that deliver 50 single-mode squeezed states from PDC [84]. Although they demonstrate high detection efficiency (63%) and high photon purity (94%), necessary to ensure high indistinguishability in the interferometer, the system has a few limiting factors. To demonstrate quantum advantage, it requires the parallel generation of a large number of highly squeezed modes, drastically increasing the number of squeezers. In this sense, integrated squeezing sources are more suitable than bulk devices. In terms of scalability, PICs can reduce the footprint of the photonic quantum hardware, not only by miniaturizing the processor but also by integrating more components on the same chip. In these systems, it is also possible to change the setting of the interferometer by remotely controlling the phase shifters, thereby enabling its reconfigurability, a property that is lacking in most bulk circuits [33, 84]. An example of GBS from PICs is shown in Ref. [28], where four SiN

microring resonators have been used to generate four pairs of two-mode squeezed states, then converted into single-mode squeezing in the first stage of the programmable integrated interferometer. In fact, if the two paired modes are sent as input to a beam splitter, the output modes are in two single-mode squeezed states [5].

On the other hand, squeezed states are not only used directly as qumodes, but they are also implemented for the generation of more complex states. A quantum computer, to be universal, requires the use of non-Gaussian states and operations, and squeezed states can be used to create such states. In particular, GBS devices can be used to generate Gottesman-Kitaev-Preskill (GKP) states [89]. Recently, a hybrid architecture that combines squeezed and GKP states has been proposed by Ref. [90], where they infer that the minimum level of squeezing necessary to generate the GKP states with high fidelity is around 10 dB. State-of-the-art integrated devices have already demonstrated the ability to deliver on-chip such a level of squeezing [44]. However, the higher the squeezing level, the more resilient the system is to loss and errors. A simplified version of this machine has recently been realized employing 21 SiN PICs that generate 86 two-mode vacuum squeezed modes [32]. However, its performance in terms of losses needs to be improved by 20-30 times to reach fault-tolerant quantum computation.

4.3.2 Quantum communication

Another possible application of squeezed states in quantum information processing is in the implementation of quantum teleportation used in CV quantum communication and networking schemes [5].

In CV quantum communication, the information is encoded in the continuous quadratures of quantum modes. A typical teleportation protocol is based on the use of two-mode quadrature vacuum squeezing, where the sender and the receiver own one of the signal and idler modes each. The quantum correlations that link these modes together are the key ingredient necessary to transfer the quantum information encoded in a third mode. The latter is made overlap with the squeezed mode of the sender, which communicates the results of homodyne measurements to the receiver via a classical channel. Based on this information, the receiver is able to displace and rotate its squeezed mode to recreate the original third mode of the sender [91, 92]. A relevant quantity that indicates the quality of the procedure is the no-cloning fidelity, which describes the minimum fidelity of the teleported state that ensures nobody

else has a better copy than the receiver. This fidelity strongly depends on the level of squeezing of the two-mode state, and a minimum of 3 dB of squeezing is required to reach the non-cloning fidelity [93].

This protocol can be extended to build quantum networks by distributing multipartite entanglement between several nodes, obtained from the connection of two or more nodes via multimode squeezed states [91], delivered, for example, from squeezed quantum combs.

4.3.3 Quantum sensing

Squeezed states find their natural application in the field of sensing and metrology because of the possibility to go beyond the standard quantum limit of noise imposed on classical light and increase the signal-to-noise ratio (SNR). When light is used to probe a sample, the information is encoded in a given property of the field, such as its amplitude or phase. The sensitivity of the measurement, which is related to the minimum measurable quantity, can be reduced by probing with the appropriate quadrature squeezed state [21].

Similar benefits in terms of sensitivity can be achieved by increasing the beam power. However, there is a limit to how much power can be delivered in or handled by a system. For example, the use of amplitude squeezed vacuum light is particularly useful in sensing biological samples, where high power light is avoided to prevent any damage of the samples. A single-mode probe with 6 dB of vacuum amplitude squeezing allowed for the demonstration of almost 2.4 dB of quantum noise reduction [94].

In case of measurements that involve the use of interferometers, vacuum squeezed states can be injected into the open port to replace the vacuum noise that would otherwise enter the system [9]. The choice of the correct squeezed state, depending on the measured quantity, is fundamental to actually attenuating the measurement noise and not amplifying it. For example, this approach, based on the injection of single-mode vacuum squeezing into the dark port of the interferometer, was implemented at LIGO for the detection of gravitational waves. They have improved the sensitivity of the detectors over a broad frequency range by using frequency-dependent squeezed light. Phase quadrature vacuum squeezed states are rotated via a filter cavity following the response of the interferometer, thereby compensating for shot noise at high frequencies and radiation pressure at low frequencies [19, 20].

In general, the intensity of a squeezed vacuum state is too low to be detected and used directly as the probing signal. The noise reduction

intrinsic to the squeezed light must be transferred into detectable coherent light, making bright squeezed states the best candidate in sensing applications [21]. In particular, intensity difference squeezing has been used in some experiments in which one mode of the two-mode squeezed state is used as the probe while the other acts as the reference beam. A differential detection scheme takes advantage of the shared noise reduction property to increase the sensitivity of the measurement [95, 96]. For example, more than 3 dB of improved sensitivity has been achieved with 6.5 dB of intensity difference squeezing generated in an atomic cell [97].

Another type of squeezing employed in sensing devices are the squeezed frequency combs, such as those generated from Kerr nonlinearity, recently used to improve the sensitivity of the dual comb spectroscopy [22, 24]. Here, one frequency comb interferes with the sample under investigation while the other comb is used as a reference. The interfering pattern resulting from their heterodyne detection encodes all the information about the sample. By replacing just one of the combs with a Kerr squeezed comb, almost 3 dB of improvement in the SNR has been observed, resulting in a two-fold quantum speed-up of the measurement time [25]. Similar results can also be obtained by means of a quantum frequency comb. A theoretical analysis shows that around 10 dB of two-mode quadrature squeezing is necessary to have significant quantum advantages [23].

Chapter 5

Kerr nonlinear microresonators

The results presented in this thesis describe squeezed states generated in integrated microring resonators through the third-order nonlinearity of the SiN waveguides. This Chapter is mainly focused on describing the basic linear properties of this type of OPO and a standard approach used to model its nonlinear behavior, i.e., the Ikeda map. The latter is typically implemented in semi-classical simulations of the dynamics of a microresonator for the generation of frequency combs [98–100], and it represents the basis of the semi-classical approach used in Paper B for the squeezing simulations.

5.1 Linear dynamics

A microring resonator is a looped waveguide placed in proximity of a straight bus waveguide [101]. A simple schematic is shown in Fig. 5.1a). Due to the typical small gap between the bus and the ring, light is periodically exchanged between them as a result of the interaction of their evanescent fields. Once the light enters the ring, it remains trapped there for a certain time before being coupled out. The coupling region is considered to be point-like, and it can be described by the coupled equations typical of a beam splitter [102]

$$\begin{bmatrix} E_{out} \\ E_2 \end{bmatrix} = \begin{bmatrix} r & t \\ -t^* & r^* \end{bmatrix} \begin{bmatrix} E_{in} \\ E_1 \end{bmatrix}. \tag{5.1}$$

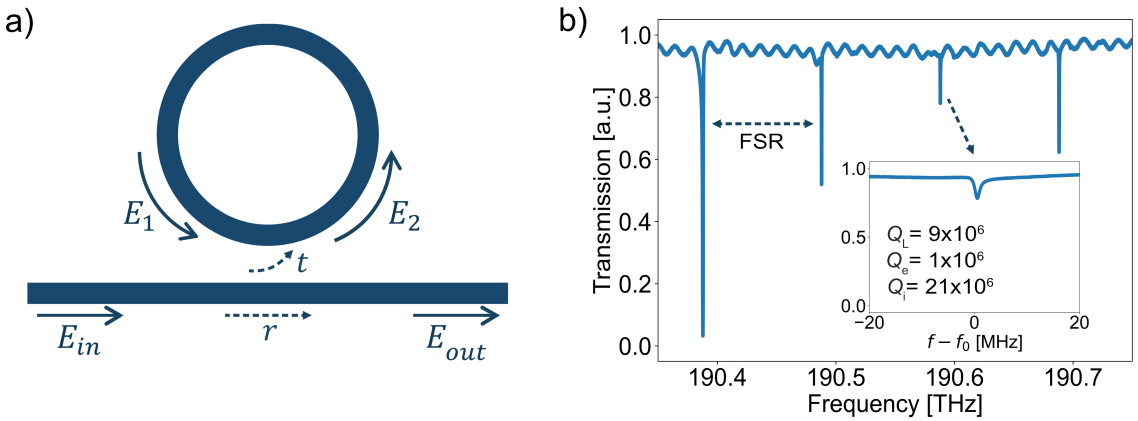

Figure 5.1: a) Schematic of a microring resonator. b) Normalized transmission spectrum measured from a microresonator pumped at low power. The insert shows the shape and quality factors of strongly overcoupled resonance.

Here, $r = |r|$ and $t = |t|e^{i\psi}$ are the reflection and transmission coefficients, with relative phase $\psi = \pi$ and that satisfy the relation $|r|^2 + |t|^2 = 1$. Moreover, E_{in} and E_{out} are the input and output fields, while E_1 and E_2 refer to the intracavity fields at two different positions of the ring, related by

$$E_1 = E_2 e^{(-\alpha_p/2 + i\beta)L}. \tag{5.2}$$

This equation describes that, during propagation in one roundtrip in a ring of length L, the field is subject to propagation loss, which is described by the coefficient per unit length α_p, and it accumulates a certain phase, proportional to the propagation constant β.

In a dispersive medium, β is frequency-dependent, affecting the conditions of operation of the microresonator. In particular, it determines the phase-matching condition of a nonlinear process. Its Taylor expansion, up to the second order, is

$$\beta(\omega - \omega_0) = \beta_0 + \beta_1(\omega - \omega_0) + \frac{\beta_2}{2!}(\omega - \omega_0)^2 + ... \tag{5.3}$$

Here, β_0 describes the phase velocity, β_1 defines the group velocity as $v_g = 1/\beta_1$, and β_2 describes the group velocity dispersion. If positive, the low-frequency components travel faster and the dispersion is referred to as normal. On the contrary, if β_2 is negative, the high frequencies are faster and the dispersion is anomalous.

Eq.5.1 and 5.2 define the linear dynamics of the microresonator, which is described by the transmission spectrum $T = |E_{out}|^2/|E_{in}|^2$.

In the lab, we usually characterize the linear cavity properties by implementing swept wavelength interferometry at low power to prevent the occurrence of nonlinear processes [103]. An example of a portion of the measured transmission spectrum is shown in Fig. 5.1b). It presents resonance dips located at the longitudinal modes of the resonator, whose positions are defined by $\beta(\omega)L = 2\pi\mu$, where μ is the integer mode number. The separation between adjacent resonances is the free spectral range (FSR), which is not constant over a broad frequency range due to the dispersion.

The resonances have a Lorentzian shape, whose width and depth depend on the total cavity losses, usually expressed in terms of the loaded quality factor

$$Q_{\mathrm{L}} = \frac{\omega_0}{\omega_{FWHM}}, \tag{5.4}$$

where ω_0 is the resonance frequency, and ω_{FWHM} is its full width at half maximum. This quality factor represents the number of field oscillations necessary for the light energy to be reduced to $1/e$ of its initial value. It has two main contributions $Q_{\mathrm{L}}^{-1} \approx Q_{\mathrm{e}}^{-1} + Q_{\mathrm{i}}^{-1}$. One comes from the coupling loss, described by the extrinsic quality factor

$$Q_{\mathrm{e}} = \frac{\omega_0 n_g L\sqrt{r}}{2(1-r)c_0}, \tag{5.5}$$

and one from the propagation loss, described by the intrinsic quality factor

$$Q_{\mathrm{i}} = \frac{\omega_0 n_g L\sqrt{a}}{2(1-a)c_0}. \tag{5.6}$$

Here, n_g is the group index, c_0 is the speed of light in vacuum, and $a^2 = e^{-\alpha_p L}$ is the roundtrip attenuation factor. As shown in the insert of Fig. 5.1b), in the case of a strongly overcoupled resonance, ideal for squeezing generation, we have $Q_{\mathrm{e}} \ll Q_{\mathrm{i}}$, indicating that the propagation loss is smaller than the coupling loss. In this case, the resonance dip is very shallow. When the propagation and coupling coefficients are equal, the resonance is critically coupled; instead, if the propagation loss is dominant, the resonance is undercoupled. By assuming the propagation loss fixed by the fabrication process, the coupling regime is defined by adjusting the gap between the microring and the bus waveguide.

5.2 Ikeda map

The Ikeda map is a system of equations used to describe the propagation of light in a microring resonator during a large number of roundtrips. In particular, during each roundtrip in a nonlinear microring, the map is obtained considering two separate steps: the evolution of the field inside the ring, and the coupling between the ring and the bus waveguide [100, 104].

Within each roundtrip n, the evolution of the slowly varying field envelope A_n in a single transverse mode propagating in the z-direction of a nonlinear medium is described by the perturbed nonlinear Schrödinger equation (NLSE) [53]

$$\frac{\partial A_n}{\partial z} = -\frac{\alpha_p}{2} A_n + i\beta_0 A_n - \frac{i\beta_2}{2}\frac{\partial^2 A_n}{\partial t^2} + i\gamma |A_n|^2 A_n, \tag{5.7}$$

which includes the effect of propagation loss, dispersion, and Kerr nonlinearity. The strength of the nonlinear processes is commonly described by the nonlinear parameter γ, which depends on the $\chi^{(3)}$ susceptibility of the material. In a typical SiN waveguide, it is about $1\,(\mathrm{Wm})^{-1}$.

The in-out coupling equations, derived from the matrix in Eq.5.1, are

$$A_{out} = A_{in}\sqrt{1-\theta_c} - A_n\sqrt{\theta_c} \tag{5.8}$$

$$A_{n+1} = A_{in}\sqrt{\theta_c} + A_n\sqrt{1-\theta_c}, \tag{5.9}$$

where we assume $|t| = \sqrt{\theta_c}$ and $|r| = \sqrt{1-\theta_c}$.

Eqs.5.7, 5.8, and 5.9 together form the Ikeda map, which can be readily implemented in a simulation tool. In particular, the NLSE can be implemented using the split-step method [53]. Here, the field propagation is divided into small steps, where the effects of the linear and nonlinear terms are treated separately and alternated with each other.

One advantage of this approach is that it allows the introduction of several noise terms in the system and the analysis of their effect on the field evolution [99]. Most relevant for this thesis is the introduction of quantum noise, modeled as an additional field propagating with A_{in} and having a random phase and amplitude with variance equal to the shot noise. The latter is defined as $\sqrt{\hbar\omega\delta f/2}$, where $\delta f = FSR$ is the frequency resolution within one roundtrip [98].

Chapter 6

Summary and future outlook

In this thesis, we discussed several ways of generating different types of squeezed states, with more emphasis on the use of an integrated microring resonator operated as an OPO. In particular, Paper A describes the experimental analysis of intensity difference squeezing obtained from an engineered strongly overcoupled microresonator, while Paper B shows the possibility of using a semi-classical simulation tool to simulate two-mode quadrature squeezing. In future work, it would be interesting to combine these results by extending the simulations to other types of squeezed states and measuring quadrature squeezing.

In particular, the semi-classical simulations represent a unique opportunity to properly investigate the role in squeezing generation of several classical noise sources that are known to affect the classical behavior of the microresonators [99]. Therefore, a future step would be to extend the current approach to this analysis and also adapt it to the generation of other squeezed states.

From an experimental point of view, instead, it would be interesting to investigate the squeezing properties of the below-threshold modes in comb states generated above threshold. In particular, we could explore the generation of multimode squeezed states in soliton crystals, which has been theoretically predicted in previous studies [80]. This analysis could be performed by adapting classical measurement techniques developed in the group, such as dual comb interference, to the quantum regime. With this work, we could contribute to understanding the role of quantum processes in the formation of classical comb states, whose investigation has mostly been restricted to the classical properties. Moreover, exploring new ways to generate multimode squeezed states could be ben-

eficial in applications that, for example, require the creation of squeezed or entangled cluster states, like quantum computing or communication.

Chapter 7

Summary of Papers

Paper A

Intensity difference squeezing of high-power modes in a strongly overcoupled silicon nitride microresonator,
Submitted to Optics Letters, 2026.

In this work, we investigate the advantages of generating intensity difference squeezing using an engineered microring resonator based on quasi-bound states in the continuum. The periodic strongly overcoupled resonances arising in this device allow for reaching a high level of on-chip squeezing, surpassing the performance of previous integrated sources. We show that this coupling regime ensures the suppression of mode competition at high input pump power, resulting in high-power squeezed twin beams.

My contribution: I conducted the experiment and the data analysis. I wrote the paper with support from the co-authors.

Paper B

Semi-classical analysis of two-mode quadrature squeezing in a high-Q microresonator,
Submitted to Conference on Lasers and Electro-Optics (CLEO), 2026.

Here, we demonstrate that the semi-classical simulation approach based on the Ikeda map, typically employed to analyze the classical

nonlinear dynamics of microring resonators, can also be used to simulate two-mode quadrature vacuum squeezing. We discuss the benefits of using this approach, which include direct access to the evolution of the entire quantum frequency combs, and the possibility of accurately implementing several classical noise sources in the model in order to analyze their effect on the squeezing level.

My contribution: I did the simulations. I wrote the manuscript with support from the co-authors.

Chapter 8

Appendices

Appendix A – Free-space experimental setup for intensity difference squeezing generation

In this section, we discuss important aspects of the experimental setup used in Paper A for the generation and characterization of intensity difference squeezing. A simplified schematic is shown in Fig. 8.1a). In order to measure this type of squeezing, we need to pump the microring resonator above the parametric threshold until strong mode pairs are generated. Then, the signal and idler beams are sent separately to the two input ports of the balanced photodetector (BPD) (Thorlabs PDB425C-AC). The noise of the photocurrent difference is then analyzed with an ESA (Anritsu MS2840A) and compared with the shot noise.

To reduce the setup losses that drastically affect the measurable level of squeezing, we use free-space components between the chip and the BPD. This is done mainly for two reasons: to reduce the loss in coupling the light out of the chip, and to optimize the spatial separation of the twin beams. A close look at the free-space setup is given by Fig. 8.1b).

The first step of squeezing generation is done by sending an amplified CW laser (Toptica CLT) into the chip using a lensed fiber, whose alignment is optimized by maximizing the output power collected with a second lensed fiber. Then, the output fiber is replaced with an aspheric lens (C330TMD-C) with a high numerical aperture capable of collecting the divergent beam coming from the tapered waveguide. After coupling, the frequency of the laser is tuned with the incorporated piezo controller to pump one strongly overcoupled resonance. The output spectrum is monitored with an OSA (Yokogawa AQ6375B).

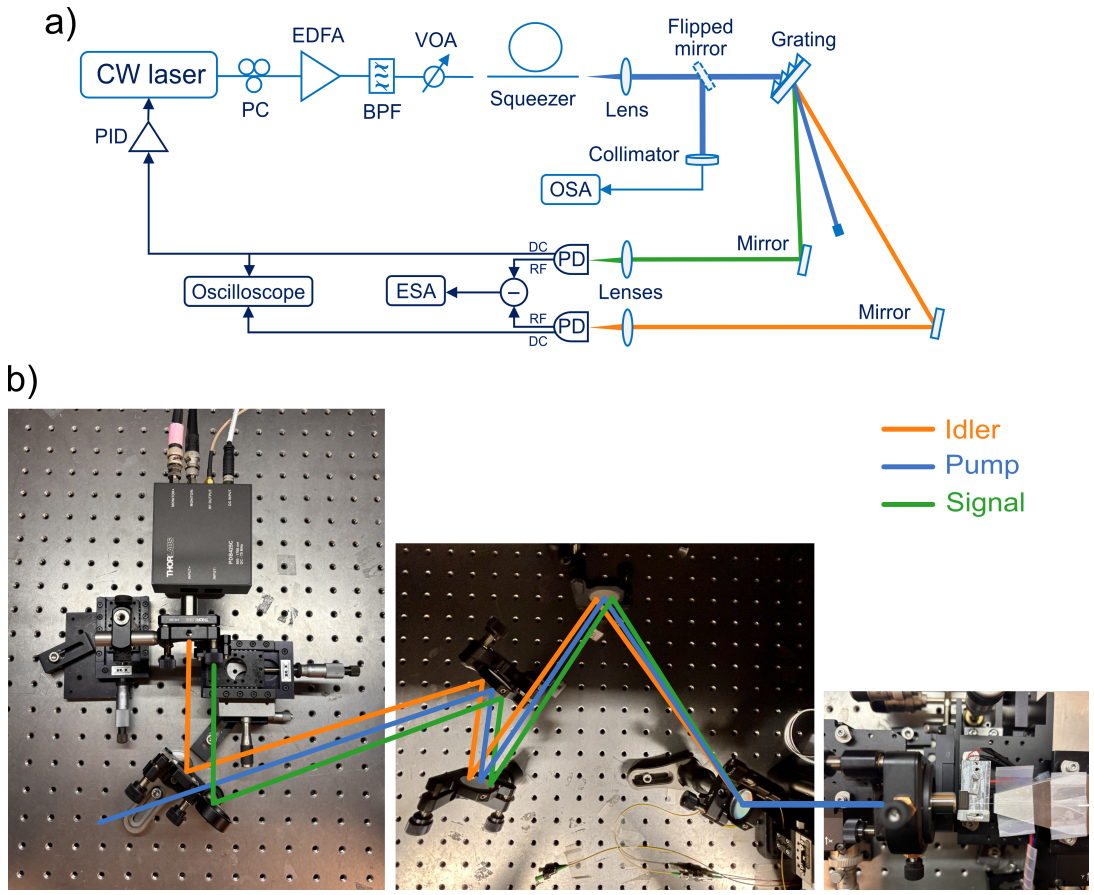

Figure 8.1: a) Schematic of the experimental setup. CW laser: continuous-wave laser; PC: polarization controller; EDFA: erbium-doped fiber amplifier; BPF: optical band pass filter; VOA: variable optical attenuator; OSA: optical spectrum analyzer; PD: photodetector; ESA: electrical spectrum analyzer; PID: proportional-integral-derivative control. b) Pictures of the free-space component, highlighting the path of the pump (blue), signal (green), and idler (orange) beams from the chip (right) to the photodetector (left).

Once the signal and idler beams are generated, we spatially separate them by using a polarization-insensitive transmission grating (GP1006Z) and a series of protected silver mirrors (PF10-03-P01). Then, two lenses (AC080-010-ML and LA1304-C-ML) focus the signal and the idler into the input ports of the BPD. The DC voltage of one of the output monitor ports is used as the error signal of the PID control box of the laser for power stabilization during the noise measurement.

To properly characterize the intensity difference squeezing, the output photocurrents need to be balanced. This is done by monitoring the two DC output signals with an oscilloscope and adjusting the system alignment to reduce the power of the most intense beam until the two

signals are equal. When the two signals are well balanced, the noise power in the ESA is minimized. Therefore, a high precision in the alignment is necessary to optimize the squeezing measurement.

Appendix B – Shot noise characterization

Here, we briefly describe the procedure implemented to characterize the shot noise used as the reference in the intensity difference squeezing analysis. In this case, the shot noise corresponds to the noise power of the laser set at the pump frequency, and whose power is the average of the signal and idler power levels. The CW laser, the BPD, and the ESA used in this characterization must be the same as those used to measure the noise power of the signal and idler.

Fig. 8.2a) shows a schematic of the experimental setup. The input laser is split evenly into two paths towards the two input ports of the BPD. Two VOAs are used to independently control the power levels of the signal and idler beams. As described previously, we need to balance the two photcurrents. To do so, we equalize the voltages from the monitor ports by adjusting the input powers. The target voltage level should be the same as that used in the squeezing measurement. Finally, the shot noise level is measured on the ESA.

An additional important test to do is to check if the laser and the detection systems are shot noise limited. In that regime, according to Eq.2.7, the shot noise varies linearly with the optical pump power. This linear dependence can be easily checked by sweeping the input pump power and observing the output noise power, as shown in Fig. 8.2b).

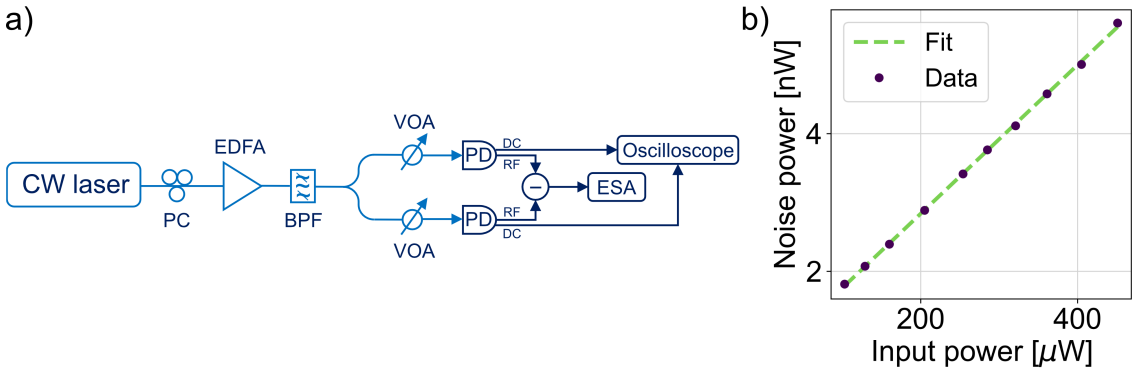

Figure 8.2: a) Schematic of the experimental setup used for the characterization of the shot noise. b) Linear dependence of the measured noise on the input power.

References

[1] M. O. Scully and M. S. Zubairy, *Quantum Optics*. Cambridge University Press, 1997.

[2] Z. Ou, *Quantum optics for experimentalists*. World Scientific Publishing Co. Pte Ltd, 2017.

[3] Z. Y. Ou, "Fundamental quantum limit in precision phase measurement," *Phys. Rev. A*, vol. 55, pp. 2598–2609, 1997.

[4] M. Teich and B. Saleh, "Squeezed states of light," *Quantum Optics Journal of the European Optical Society Part B*, vol. 1, pp. 153–191, 1989.

[5] A. I. Lvovsky, *Squeezed Light*. John Wiley Sons, Ltd, 2015, ch. 5, pp. 121–163.

[6] D. Stoler, "Equivalence classes of minimum uncertainty packets," *Phys. Rev. D*, vol. 1, pp. 3217–3219, 1970.

[7] E. Lu, "New coherent states of the electromagnetic field," *Lettere al Nuovo Cimento*, vol. 2, pp. 1241–1244, 1971.

[8] H. P. Yuen, "Two-photon coherent states of the radiation field," *Phys. Rev. A*, vol. 13, pp. 2226–2243, 1976.

[9] C. M. Caves, "Quantum-mechanical noise in an interferometer," *Physical Review D*, vol. 23, pp. 1693–1708, 1981.

[10] D. F. Walls, "Squeezed states of light," *Nature*, vol. 306, pp. 141–146, 1983.

[11] R. E. Slusher, L. W. Hollberg, B. Yurke, J. C. Mertz, and J. F. Valley, "Observation of squeezed states generated by four-wave mixing in an optical cavity," *Phys. Rev. Lett.*, vol. 55, pp. 2409–2412, 1985.

[12] P. K. Lam, T. C. Ralph, B. C. Buchler, D. E. McClelland, H.-A. Bachor, and J. Gao, "Optimization and transfer of vacuum squeezing from an optical parametric oscillator," *Journal of Optics B: Quantum and Semiclassical Optics*, vol. 1, no. 4, p. 469, 1999.

[13] S. Suzuki, H. Yonezawa, F. Kannari, M. Sasaki, and A. Furusawa, "7db quadrature squeezing at 860nm with periodically poled ktiopo4," *Applied Physics Letters*, vol. 89, no. 6, p. 061116, 2006.

[14] Y. Takeno, M. Yukawa, H. Yonezawa, and A. Furusawa, "Observation of -9 db quadrature squeezing with improvement of phase stability in homodyne measurement," *Opt. Express*, vol. 15, no. 7, pp. 4321–4327, 2007.

[15] H. Vahlbruch, M. Mehmet, S. Chelkowski, B. Hage, A. Franzen, N. Lastzka, S. Goßler, K. Danzmann, and R. Schnabel, "Observation of squeezed light with 10-db quantum-noise reduction," *Phys. Rev. Lett.*, vol. 100, p. 033602, 2008.

[16] M. Mehmet, S. Ast, T. Eberle, S. Steinlechner, H. Vahlbruch, and R. Schnabel, "Squeezed light at 1550 nm with a quantum noise reduction of 12.3 db," *Opt. Express*, vol. 19, no. 25, pp. 25 763–25 772, 2011.

[17] G. Sim, H. Kim, and H. S. Moon, "Intensity-difference squeezing from four-wave mixing in hot 85rb and 87rb atoms in single diode laser pumping system," *Scientific Reports*, vol. 15, p. 7727, 2025.

[18] H. Vahlbruch, M. Mehmet, K. Danzmann, and R. Schnabel, "Detection of 15 db squeezed states of light and their application for the absolute calibration of photoelectric quantum efficiency," *Physical Review Letters*, vol. 117, p. 110801, 2016.

[19] D. Ganapathy and et al., "Broadband quantum enhancement of the ligo detectors with frequency-dependent squeezing," *Physical Review X*, vol. 13, p. 041021, 2023.

[20] W. Jia and et al., "Squeezing the quantum noise of a gravitational-wave detector below the standard quantum limit," *Science*, vol. 385, pp. 1318–1321, 2024.

[21] B. J. Lawrie, P. D. Lett, A. M. Marino, and R. C. Pooser, "Quantum sensing with squeezed light," *ACS Photonics*, vol. 6, pp. 1307–1318, 2019.

[22] N. Kalinin, T. Dirmeier, A. A. Sorokin, E. A. Anashkina, L. L. Sánchez-Soto, J. F. Corney, G. Leuchs, and A. V. Andrianov, "Quantum-enhanced interferometer using kerr squeezing," *Nanophotonics*, vol. 12, pp. 2945–2952, 2023.

[23] H. Shi, Z. Chen, S. E. Fraser, M. Yu, Z. Zhang, and Q. Zhuang, "Entanglement-enhanced dual-comb spectroscopy," *npj Quantum Information*, vol. 9, 2023.

[24] A. Belsley, "Quantum-enhanced absorption spectroscopy with bright squeezed frequency combs," *Physical Review Letters*, vol. 130, p. 133602, 2023.

[25] D. I. Herman, M. Walsh, M. K. Kreider, N. Lordi, E. J. Tsao, A. J. Lind, M. Heyrich, J. Combes, J. Genest, and S. A. Diddams, "Squeezed dual-comb spectroscopy," *Science*, 2025.

[26] S. L. Braunstein, "Squeezing as an irreducible resource," *Physical Review A*, vol. 71, p. 055801, 2005.

[27] L. S. Madsen, F. Laudenbach, M. F. Askarani, F. Rortais, T. Vincent, J. F. Bulmer, F. M. Miatto, L. Neuhaus, L. G. Helt, M. J. Collins, A. E. Lita, T. Gerrits, S. W. Nam, V. D. Vaidya, M. Menotti, I. Dhand, Z. Vernon, N. Quesada, and J. Lavoie, "Quantum computational advantage with a programmable photonic processor," *Nature*, vol. 606, pp. 75–81, 2022.

[28] J. M. Arrazola and et al., "Quantum circuits with many photons on a programmable nanophotonic chip," *Nature*, vol. 591, pp. 54–60, 2021.

[29] S. Takeda and A. Furusawa, "Toward large-scale fault-tolerant universal photonic quantum computing," *APL Photonics*, vol. 4, p. 060902, 2019.

[30] S. L. Braunstein and P. V. Loock, "Quantum information with continuous variables," Tech. Rep., 2005.

[31] J. E. Bourassa, R. N. Alexander, M. Vasmer, A. Patil, I. Tzitrin, T. Matsuura, D. Su, B. Q. Baragiola, S. Guha, G. Dauphinais, K. K. Sabapathy, N. C. Menicucci, and I. Dhand, "Blueprint for a scalable photonic fault-tolerant quantum computer," *Quantum*, vol. 5, p. 392, 2021.

[32] H. Aghaee Rad, T. Ainsworth, R. Alexander, B. Altieri, M. Askarani, R. Baby, L. Banchi, B. Baragiola, J. Bourassa, R. Chadwick *et al.*, "Scaling and networking a modular photonic quantum computer," *Nature*, pp. 1–8, 2025.

[33] J. Wang, F. Sciarrino, A. Laing, and M. G. Thompson, "Integrated photonic quantum technologies," *Nature Photonics*, vol. 14, pp. 273–284, 2020.

[34] H. S. Stokowski, T. P. McKenna, T. Park, A. Y. Hwang, D. J. Dean, O. T. Celik, V. Ansari, M. M. Fejer, and A. H. Safavi-Naeini, "Integrated quantum optical phase sensor in thin film lithium niobate," *Nature Communications*, vol. 14, p. 3355, 2023.

[35] T. Park, H. Stokowski, V. Ansari, S. Gyger, K. K. S. Multani, O. T. Celik, A. Y. Hwang, D. J. Dean, F. Mayor, T. P. Mckenna, M. M. Fejer, and A. Safavi-Naeini, "Single-mode squeezed-light generation and tomography with an integrated optical parametric oscillator," *Sci. Adv*, vol. 10, p. 1814, 2024.

[36] X. Shi, A. A. Baiju, X. Chen, S. S. Mohanraj, S. Wang, V. Dhyani, B. Shajilal, M. Zhao, R. Yang, Y. Li, G. Wu, H. Hao, V. Leong, P. K. Lam, and D. Zhu, "Squeezed light generation in periodically poled thin-film lithium niobate waveguides," *http://arxiv.org/abs/2508.08599*, 2025.

[37] A. Dutt, K. Luke, S. Manipatruni, A. L. Gaeta, P. Nussenzveig, and M. Lipson, "On-chip optical squeezing," *Physical Review Applied*, vol. 3, p. 044005, 2015.

[38] V. D. Vaidya, B. Morrison, L. G. Helt, R. Shahrokshahi, D. H. Mahler, M. J. Collins, K. Tan, J. Lavoie, A. Repingon, M. Menotti, N. Quesada, R. C. Pooser, A. E. Lita, T. Gerrits, S. W. Nam, and Z. Vernon, "Broadband quadrature-squeezed vacuum and nonclassical photon number correlations from a nanophotonic device," *Science Advances*, vol. 6, no. 39, p. eaba9186, 2020.

[39] Y. Zhang, M. Menotti, K. Tan, V. D. Vaidya, D. H. Mahler, L. G. Helt, L. Zatti, M. Liscidini, B. Morrison, and Z. Vernon, "Squeezed light from a nanophotonic molecule," *Nature Communications*, vol. 12, p. 2233, 2021.

[40] M. Jahanbozorgi, Z. Yang, S. Sun, H. Chen, R. Liu, B. Wang, and X. Yi, "Generation of squeezed quantum microcombs with silicon nitride integrated photonic circuits," *Optica*, vol. 10, p. 1100, 2023.

[41] T. Kashiwazaki, T. Yamashima, N. Takanashi, A. Inoue, T. Umeki, and A. Furusawa, "Fabrication of low-loss quasi-single-mode ppln waveguide and its application to a modularized broadband high-level squeezer," *Applied Physics Letters*, vol. 119, 2021.

[42] Y. Shen, P.-Y. Hsieh, S. K. Sridhar, S. Feldman, Y.-C. Chang, T. A. Smith, and A. Dutt, "Strong nanophotonic quantum squeezing exceeding 3.5db in a foundry-compatible kerr microresonator," *Optica*, vol. 12, p. 302, 2025.

[43] Y. Shen, P.-Y. Hsieh, D. Srinivasan, A. Henry, G. Moille, S. K. Sridhar, A. Restelli, Y.-C. Chang, K. Srinivasan, T. A. Smith, and A. Dutt, "Highly squeezed nanophotonic quantum microcombs with broadband frequency tunability," *http://arxiv.org/abs/2505.03734*, 2025.

[44] Z. Yang, M. Jahanbozorgi, D. Jeong, S. Sun, O. Pfister, H. Lee, and X. Yi, "A squeezed quantum microcomb on a chip," *Nature Communications*, vol. 12, 2021.

[45] F. Lei, Z. Ye, K. Twayana, Y. Gao, M. Girardi, Óskar B. Helgason, P. Zhao, and V. Torres-Company, "Hyperparametric oscillation via bound states in the continuum," *Physical Review Letters*, vol. 130, p. 093801, 2023.

[46] H.-A. Bachor and T. C. Ralph, *A Guide to Experiments in Quantum Optics*. John Wiley Sons, Ltd, 2019.

[47] S. E. Dwyer and J. Belcher, "Quantum noise reduction using squeezed states in ligo," Massachusetts Institute of Technology, Tech. Rep., 2013.

[48] G. P. Agrawal, *Fiber-Optic Communication Systems*. John Wiley Sons, Ltd, 2021, ch. 4, pp. 107–150.

[49] G. Breitenbach, S. Schiller, and J. Mlynek, "Measurement of the quantum states of squeezed light," *Nature*, vol. 387, pp. 471—-475, 1997.

[50] P. Drummond and Z. Ficek, *Quantum Squeezing*, ser. Springer Series on Atomic, Optical, and Plasma Physics. Springer Berlin Heidelberg, 2013.

[51] C. Gerry and P. Knight, *Nonclassical light*. Cambridge University Press, 2010, pp. 150–194.

[52] M. C. Teich and B. E. A. Saleh, "Squeezed state of light," *Quantum Optics: Journal of the European Optical Society Part B*, vol. 1, no. 2, p. 153, 1989.

[53] G. P. Agrawal, *Nonlinear Fiber Optics*, 5th ed. Elsevier, 2012.

[54] I. Rigas, A. B. Klimov, L. L. Sánchez-Soto, and G. Leuchs, "Nonlinear cross-kerr quasiclassical dynamics," *New Journal of Physics*, vol. 15, no. 4, p. 043038, 2013.

[55] R. Dong, J. Heersink, J. F. Corney, P. D. Drummond, U. L. Andersen, and G. Leuchs, "Experimental evidence for raman-induced limits to efficient squeezing in optical fibers," *Optics Letters*, vol. 33, p. 116, 2008.

[56] P. D. Drummond, R. M. Shelby, S. R. Friberg, and Y. Yamamoto, "Quantum solitons in optical fibres," , vol. 365, no. 6444, pp. 307–313, 1993.

[57] U. L. Andersen, T. Gehring, C. Marquardt, and G. Leuchs, "30 years of squeezed light generation," *Physica Scripta*, vol. 91, 2016.

[58] T. Kashiwazaki, T. Yamashima, K. Enbutsu, T. Kazama, A. Inoue, K. Fukui, M. Endo, T. Umeki, and A. Furusawa, "Over-8-db squeezed light generation by a broadband waveguide optical parametric amplifier toward fault-tolerant ultra-fast quantum computers," *Applied Physics Letters*, vol. 122, 2023.

[59] K. Hirota, T. Kashiwazaki, G. Ha, T. Yamashima, P. Jaturaphagorn, T. Suzuki, K. Takahashi, A. Kawasaki, A. Inoue, W. Asavanant, M. Endo, T. Umeki, and A. Furusawa, "Generation of 10-db squeezed light from a broadband waveguide optical parametric amplifier with improved phase locking method," 2025.

[60] G. Ren and C.-z. Zhang, "An entangled squeezed state generated by an optical parametric amplifier and a beam splitter," *Laser Physics*, vol. 35, no. 3, p. 035202, 2025.

[61] A. Hosaka, K. Hirosawa, R. Sawada, and F. Kannari, "Generation of photon-number squeezed states with a fiber-optic symmetric interferometer," *Opt. Express*, vol. 23, no. 15, pp. 18 850–18 863, 2015.

[62] A. V. Andrianov, N. A. Kalinin, A. A. Sorokin, E. A. Anashkina, and G. Leuchs, "Fiber-optical sources of quantum squeezed light," *Optoelectronics, Instrumentation and Data Processing*, vol. 59, pp. 28–38, 2023.

[63] H. Liu, M. L. Iu, N. Hamdash, and A. S. Helmy, "Towards arbitrary time-frequency mode squeezing with self-conjugated mode squeezing in fiber," *Nature Communications*, vol. 16, no. 1, p. 6524, 2025.

[64] R. M. Shelby, M. D. Levenson, S. H. Perlmutter, R. G. DeVoe, and D. F. Walls, "Broad-band parametric deamplification of quantum noise in an optical fiber," *Phys. Rev. Lett.*, vol. 57, pp. 691–694, 1986.

[65] J. F. Corney, J. Heersink, R. Dong, V. Josse, P. D. Drummond, G. Leuchs, and U. L. Andersen, "Simulations and experiments on polarization squeezing in optical fiber," *Phys. Rev. A*, vol. 78, p. 023831, 2008.

[66] P.-K. Chen, I. Briggs, S. Hou, and L. Fan, "Ultra-broadband quadrature squeezing with thin-film lithium niobate nanophotonics," *Opt. Lett.*, vol. 47, no. 6, pp. 1506–1509, 2022.

[67] R. Nehra, R. Sekine, L. Ledezma, Q. Guo, R. M. Gray, A. Roy, and A. Marandi, "Few-cycle vacuum squeezing in nanophotonics," *Science*, vol. 377, no. 6612, pp. 1333–1337, 2022.

[68] N. Takanashi, A. Inoue, T. Kashiwazaki, T. Kazama, K. Enbutsu, R. Kasahara, T. Umeki, and A. Furusawa, "All-optical phase-sensitive detection for ultra-fast quantum computation," *Optics Express*, vol. 28, p. 34916, 2020.

[69] I. Barakat, M. Kalash, D. Scharwald, P. Sharapova, N. Lindlein, and M. Chekhova, "Simultaneous measurement of multimode squeezing through multimode phase-sensitive amplification," *Optica Quantum*, vol. 3, p. 36, 2025.

[70] Y. K. Chembo, "Quantum dynamics of kerr optical frequency combs below and above threshold: Spontaneous four-wave mixing, entanglement, and squeezed states of light," *Physical Review A*, vol. 93, p. 033820, 2016.

[71] A. E. Ulanov, B. Ruhnke, T. Wildi, and T. Herr, "Quadrature squeezing in a nanophotonic microresonator," *Nature Communications*, vol. 16, p. 10791, 2025.

[72] N. Quesada, L. G. Helt, M. Menotti, M. Liscidini, and J. E. Sipe, "Beyond photon pairs—nonlinear quantum photonics in the high-gain regime: a tutorial," *Advances in Optics and Photonics*, vol. 14, p. 291, 2022.

[73] C. M. Caves and B. L. Schumaker, "New formalism for two-photon quantum optics. i. quadrature phases and squeezed states," *Phys. Rev. A*, vol. 31, pp. 3068–3092, 1985.

[74] Y. Zhao, Y. Okawachi, J. K. Jang, X. Ji, M. Lipson, and A. L. Gaeta, "Near-degenerate quadrature-squeezed vacuum generation on a silicon-nitride chip," *Physical Review Letters*, vol. 124, p. 193601, 2020.

[75] A. Viola, F. Malaspina, and M. Liscidini, "Squeezing enhancement by suppression of noise through a resonant interferometric coupler," *Optics Letters*, vol. 49, p. 5611, 2024.

[76] T. Herr, K. Hartinger, J. Riemensberger, C. Wang, E. Gavartin, R. Holzwarth, M. Gorodetsky, and T. Kippenberg, "Universal formation dynamics and noise of kerr-frequency combs in microresonators," *Nature Photonics*, vol. 6, pp. 480–487, 2012.

[77] T. Herr, V. Brasch, J. Jost, C. Wang, N. Kondratiev, M. Gorodetsky, and T. Kippenberg, "Temporal solitons in optical microresonators," *Nature Photonics*, vol. 8, 2012.

[78] M. Kues, C. Reimer, J. M. Lukens, W. J. Munro, A. M. Weiner, D. J. Moss, and R. Morandotti, "Quantum optical microcombs," pp. 170–179, 2019.

[79] M. A. Guidry, D. M. Lukin, K. Y. Yang, R. Trivedi, and J. Vučković, "Quantum optics of soliton microcombs," *Nature Photonics*, vol. 16, pp. 52–58, 2022.

[80] M. A. Guidry, D. M. Lukin, K. Y. Yang, and J. Vučković, "Multimode squeezing in soliton crystal microcombs," *Optica*, vol. 10, p. 694, 2023.

[81] P. Tritschler, T. Ohms, C. Schweikert, O. Soezen, R. H. Klenk, S. Abdani, W. Vogel, G. Rademacher, A. Zimmermann, and P. Degenfeld-Schonburg, "Chip-integrated single-mode coherent-squeezed light source using four-wave mixing in microresonators," *arXiv preprint arXiv:2502.16278*, 2025.

[82] A. Dutt, S. Miller, K. Luke, J. Cardenas, A. L. Gaeta, P. Nussenzveig, and M. Lipson, "Tunable squeezing using coupled ring resonators on a silicon nitride chip," *Opt. Lett.*, vol. 41, no. 2, pp. 223–226, 2016.

[83] R. A. Kögler, G. C. Rickli, R. R. Domeneguetti, X. Ji, A. L. Gaeta, M. Lipson, M. Martinelli, and P. Nussenzveig, "Quantum state tomography in a third-order integrated optical parametric oscillator," *Optics Letters*, vol. 49, p. 3150, 2024.

[84] H.-S. Zhong, H. Wang, Y.-H. Deng, M.-C. Chen, L.-C. Peng, Y.-H. Luo, J. Qin, D. Wu, X. Ding, Y. Hu, P. Hu, X.-Y. Yang, W.-J. Zhang, H. Li, Y. Li, X. Jiang, L. Gan, G. Yang, L. You, Z. Wang, L. Li, N.-L. Liu, C.-Y. Lu, and J.-W. Pan, "Quantum computational advantage using photons," *Science*, vol. 370, pp. 1460–1463, 2020.

[85] L. S. Madsen, F. Laudenbach, M. F. Askarani, F. Rortais, T. Vincent, J. F. Bulmer, F. M. Miatto, L. Neuhaus, L. G. Helt, M. J. Collins *et al.*, "Quantum computational advantage with a programmable photonic processor," *Nature*, vol. 606, no. 7912, pp. 75–81, 2022.

[86] J. F. Bulmer, B. A. Bell, R. S. Chadwick, A. E. Jones, D. Moise, A. Rigazzi, J. Thorbecke, U.-U. Haus, T. Van Vaerenbergh, R. B. Patel *et al.*, "The boundary for quantum advantage in gaussian boson sampling," *Science advances*, vol. 8, no. 4, p. eabl9236, 2022.

[87] C. S. Hamilton, R. Kruse, L. Sansoni, S. Barkhofen, C. Silberhorn, and I. Jex, "Gaussian boson sampling," *Physical Review Letters*, vol. 119, 2017.

[88] Z. Vernon, N. Quesada, M. Liscidini, B. Morrison, M. Menotti, K. Tan, and J. E. Sipe, "Scalable squeezed-light source for continuous-variable quantum sampling," *Physical Review Applied*, vol. 12, 2019.

[89] M. V. Larsen, J. E. Bourassa, S. Kocsis, J. F. Tasker, R. S. Chadwick, C. González-Arciniegas, J. Hastrup, C. E. Lopetegui-González, F. M. Miatto, A. Motamedi, R. Noro, G. Roeland, R. Baby, H. Chen, P. Contu, I. D. Luch, C. Drago, M. Giesbrecht, T. Grainge, I. Krasnokutska, M. Menotti, B. Morrison, C. Puviraj, K. R. Shad, B. Hussain, J. McMahon, J. E. Ortmann, M. J. Collins, C. Ma, D. S. Phillips, M. Seymour, Q. Y. Tang, B. Yang, Z. Vernon, R. N. Alexander, and D. H. Mahler, "Integrated photonic source of gottesman–kitaev–preskill qubits," *Nature*, 2025.

[90] J. E. Bourassa, R. N. Alexander, M. Vasmer, A. Patil, I. Tzitrin, T. Matsuura, D. Su, B. Q. Baragiola, S. Guha, G. Dauphinais, K. K. Sabapathy, N. C. Menicucci, and I. Dhand, "Blueprint for a Scalable Photonic Fault-Tolerant Quantum Computer," *Quantum*, vol. 5, p. 392, 2021.

[91] S. Pirandola and S. Mancini, "Quantum teleportation with continuous variables: A survey," *Laser Physics*, vol. 16, pp. 1418–1438, 2006.

[92] S. Arora, C. Kumar, and Arvind, "Continuous-variable quantum teleportation using a photon-subtracted and photon-added two-mode squeezed coherent state," *Phys. Rev. A*, vol. 111, p. 022402, 2025.

[93] L. Sharma, P. Mudgal, S. Das, and D. Sikdar, "Enhancing squeezing to strengthen entanglement for high-fidelity quantum teleportation," *IEEE Journal of Selected Topics in Quantum Electronics*, vol. 31, 2025.

[94] M. A. Taylor, J. Janousek, V. Daria, J. Knittel, B. Hage, H. A. Bachor, and W. P. Bowen, "Biological measurement beyond the quantum limit," *Nature Photonics*, vol. 7, pp. 229–233, 2013.

[95] C. A. Casacio, L. S. Madsen, A. Terrasson, M. Waleed, K. Barnscheidt, B. Hage, M. A. Taylor, and W. P. Bowen, "Quantum-enhanced nonlinear microscopy," *Nature*, vol. 594, pp. 201–206, 2021.

[96] W. Yang, W. Diao, C. Cai, T. Wu, K. Wu, Y. Li, C. Li, C. Duan, H. Leng, N. Zi, and X. Yin, "A bright squeezed light source for quantum sensing," *Chemosensors*, vol. 11, p. 18, 2023.

[97] F. Li, T. Li, M. O. Scully, and G. S. Agarwal, "Quantum advantage with seeded squeezed light for absorption measurement," *Physical Review Applied*, vol. 15, p. 044030, 2021.

[98] R. Paschotta, "Noise of mode-locked lasers (part i): Numerical model," *Applied Physics B: Lasers and Optics*, vol. 79, 2004.

[99] F. Lei, Z. Ye, Óskar B. Helgason, A. Fülöp, M. Girardi, and V. Torres-Company, "Optical linewidth of soliton microcombs," *Nature Communications*, vol. 13, 2022.

[100] T. Hansson and S. Wabnitz, "Dynamics of microresonator frequency comb generation: models and stability," *Nanophotonics*, vol. 5, no. 2, pp. 231–243, 2016.

[101] W. Bogaerts, P. De Heyn, T. Van Vaerenbergh, K. De Vos, S. Kumar Selvaraja, T. Claes, P. Dumon, P. Bienstman, D. Van Thourhout, and R. Baets, "Silicon microring resonators," *Laser & Photonics Reviews*, vol. 6, no. 1, pp. 47–73, 2012.

[102] A. Yariv, "Universal relations for coupling of optical power between microresonators and dielectric waveguides," *Electronics Letters*, vol. 36, pp. 321–322, 2000.

[103] K. Twayana, Z. Ye, Óskar B. Helgason, K. Vijayan, M. Karlsson, and V. Torres-Company, "Frequency-comb-calibrated swept-wavelength interferometry," *Optics Express*, vol. 29, p. 24363, 2021.

[104] K. Ikeda, "Multiple-valued stationary state and its instability of the transmitted light by a ring cavity system," *Physical Review A*, vol. 30, 1979.